J. Fluid Mech. (2010), *vol.* 649, *pp.* 341–370.
doi:10.1017/S0022112009993478

Moderately three-dimensional separated and reattaching turbulent flow

J. R. HARDMAN† AND P. E. HANCOCK‡

Fluids Research Centre, Faculty of Engineering and Physical Sciences, University of Surrey, Guildford, Surrey GU2 7XH, UK

(Received 17 October 2008; revised 12 November 2009; accepted 12 November 2009)

A fully three-dimensional turbulent separated flow was set up such that it had a systematic link to two-dimensional flow, as a way of investigating the more complicated nature of this flow type. The central region of the flow was fully three-dimensional, but was bounded on its sides by regions of 'spanwise invariance' in which the flow was invariant in the lateral direction, or very nearly so. A special case of spanwise invariance, which is statistically two-dimensional, is one in which the streamlines are also coplanar, or at least nominally so in numerous experimental studies. Another aspect of the present arrangement is that the side regions should ideally provide well-defined boundary conditions. The separation was formed downstream of a doubly swept normal flat plate, forming a 'v'-shaped separation line, mounted on the front of a splitter plate, mounted in the centre of the wind tunnel working section. The predominantly inward flow to the central region implies a negative lateral strain rate ($\partial W/\partial z$), but all nine strain rates are non-zero. Measurements were made using pulsed-wire anemometry techniques for mean velocities, Reynolds stresses and wall shear stress. Even though the sweep angle is mild at $\pm 10^{\circ}$, the effect is to increase the bubble height by over 50 % in its centre to create a 'bulge', symmetrical about the centreline. The degree of three-dimensionality is described as moderate in that the peak inflow velocity from the side regions is less than 0.2 of the free-stream velocity, but comparable with the peak in the reverse-flow velocity. A larger sweep angle would give a larger inflow velocity. A separate study (Cao & Hancock, *Eur. J. Mech.* B/*Fluids*, vol. 23, 2004, p. 519) has shown that the bulge persists very far downstream, so that accurate physical modelling of the separated region is likely to be important in modelling the flow well downstream. An intermediate region exists between the invariant side region and the bulge, where all the stress levels are reduced, as would be expected from the effects of streamline convergence. Although overall there is a flow inward to the centre (streamline convergence), part of the overlying shear layer is subjected to diverging flow and an intensification of Reynolds stresses near the centre of the bulge.

1. Introduction

There have been numerous detailed studies of turbulent reattaching separated flow, experimental, numerical and analytical. These can be categorized as ones in which the separation is either from a sharp edge or from a smooth surface where the boundary

† Present address: Toyota Motorsport GmbH, Toyota-Allee 7, D-50858 Köln, Germany
‡ Email address for correspondence: P.Hancock@surrey.ac.uk

layer immediately upstream of separation is laminar, transitional or turbulent, and whether the reverse flow is weak or strong. They can also be categorized as ones in which the flow is two-dimensional, of which there are two types, or three-dimensional, and as ones in which the flow is essentially an internal flow or an external flow. Further factors include the presence of free-stream turbulence, compressibility, surface roughness, free-stream unsteadiness and so on. Most flows of practical concern are significantly even if not strongly three-dimensional, but the complexity of turbulent flows in general has meant that most attention has been confined to flows that are two-dimensional in the mean. A prime example here must be the low-speed zero-pressure-gradient turbulent boundary layer in the search for universal and incontrovertible scaling laws.

The two types of two-dimensionality are both spatially two-dimensional, but in one, one component of mean velocity W, say, is zero everywhere, and therefore all the mean streamlines lie on planes perpendicular to direction of W, so these flows might be described as 'coplanar'. A chief characteristic of this flow, which is usually associated with the term 'two-dimensional', is the invariance of all quantities in the direction of W, and leads to the other type in which W is non-zero but all quantities remain invariant in the direction of W. This latter type, three-dimensional in a restricted sense, might be described as non-coplanar two-dimensional. Both types can be described as laterally or spanwise invariant. Kaltenback & Janke (2000), who give direct numerical simulation of flow behind a swept, rearward-facing step, cite several studies.

The present flow is in the class of sharp-edge separation, with a very thin laminar boundary layer upstream of the separation line, formed by a bluff body. Its specific coplanar, two-dimensional counterparts have been studied in detail by Ruderich & Fernholz (1986), Castro & Haque (1987), Jaroch & Fernholz (1989), Hancock (2000) and Ciampoli & Hancock (2006), where the last work revisited the issue of the conditions necessary for negligible end effects. In these studies the separated flow was strong in Fernholz' classification (Fernholz 1994). Di Mare & Jones (2003) compare large eddy simulation predictions, assuming spanwise invariance in the lateral boundary conditions, with the spanwise-invariant measurements of this study, with good overall agreement. A prime intention in the work here is to provide an improved understanding of the physics of three-dimensional separated flow in which the flow is predominantly stress driven. A directly related intention is to provide a basis for testing and improving physical models.

The flow in this study (Hardman 1998) was formed behind a doubly swept separation line, as shown in figures 1 and 2 where, conceptually, the overall width is sufficient for flow either side of the central 'v' region to be spanwise invariant. Further out, the flow is affected by the presence of the wind tunnel sidewalls, as can be seen in the surface streamlines of figure 2. The flow in the central region is fully three-dimensional, but the strength of the three-dimensionality decreases with increasing distance from the centreline until it has reached that in the very nearly invariant 'side' regions. Such a flow which, incidentally, appears to be symmetrical about the centreline, provides a canonical type of flow in that it provides a systematic extension of the special case of spanwise-invariant flow, of which the coplanar flow is an even more specialized case. Another feature of the presence of the spanwise-invariant regions is that they should provide well defined boundary conditions for both time-averaged and time-resolved calculations, avoiding the need to consider the complex interactions with the wind tunnel sidewall boundary layers.

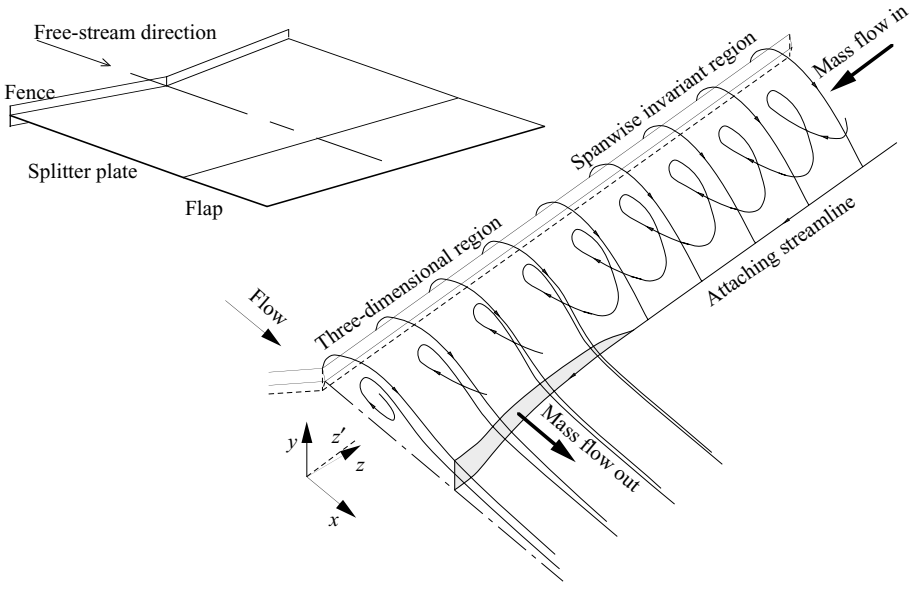

FIGURE 1. Illustration of rig and sketch of streamlines.

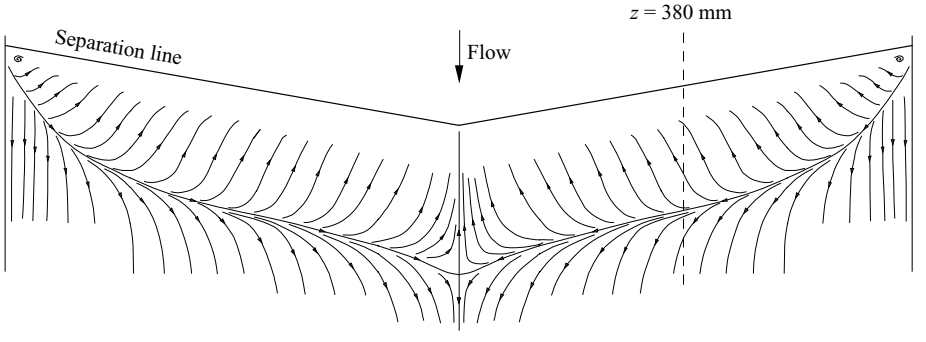

FIGURE 2. Surface streamlines on splitter plate.

Now although a flow geometry might be two-dimensional it is not always the case that the time-averaged flow is two-dimensional. (One example is that of the wide-angle symmetrical diffuser in which the flow separates from one diffuser wall and not the other.) The idea of using spanwise-invariant regions stemmed from other work which exhibited spanwise-invariance provided the flow width was large enough for end effects to have become negligible. These other sources include Sutton, Devenport & Barkey Wolf (1991) and Hancock & McCluskey (1996), and also confirmed in the work of Cao (2002) and Cao & Hancock (2004). Thus, it is expected that had the present flow been made wider still, all else constant, the extent of the region of spanwise invariance would also have been wider. The experiments of Sutton *et al.* (1991) also found the flow to be very sensitive to small imperfections in the edge of their bluff thick plate, and the same was found by Cao (2002), the former finding the sensitivity to be larger at higher sweep angles (up to the highest tested of 45°). This suggests that in some instances the absence of invariance might have been caused by imperfections in the experimental rig or flow quality.

A spanwise-invariant flow, as in the 'side regions' of figures 1 and 2, has a crossflow component (as is straightforward to argue), so that there is an 'inflow' into the central region from the sides. As a consequence the height of the separated flow is larger in this central region where, as will be seen, the lateral extent of this enlarged bubble is comparable with its height, giving the bubble a bulge-like appearance. The use of the word 'moderate' in the title of this paper is based on the inflow velocity being an order of magnitude smaller then the free-stream velocity, but with an increase in bubble height of order unity. In a spanwise-invariant flow time-averaged separating streamlines are also reattaching streamlines, but this is not the case in general, so that for the flow here the time-mean separating streamlines in the central region do not reattach but remain above the surface, marking out this bulge. However, a line of attachment exists and so the free-shear layer that bounds the outer part of the separated region can be said to reattach. Arguably, the term separation bubble only makes sense if, in a time-averaged sense, the separating streamlines are also reattaching streamlines, so that the (time-averaged) flow beneath the stream surface (formed from the separation streamlines) remains separate from that above. Nevertheless, it is convenient still to use this term as a short-hand for a flow that reattaches. For a more detailed discussion for streamline topology see Perry & Fairlie (1974).

Cao (2002) and Cao & Hancock (2004) investigated the same type flow as that here, except that the separation lines were swept at larger angles, of $\pm 25^{\circ}$ (and that it was formed on a bluff thick plate). The purpose of that work was to study the flow as it developed to distances well downstream of reattachment, the bluff plate providing an easy way to generate the smaller separation bubble needed to obtain the required relative development distance in the wind tunnel used. A larger sweep angle than that here was used to give a stronger degree of three-dimensionality and a more distinctive downstream flow. However, there is no reason to believe that the general observations would have been different had a smaller sweep angle been used. They found the bulge to be very persistent, its size and relative shape changing little in 23 reattachment lengths, and suggested it would require a distance an order of magnitude longer before the bulge disappeared into the background of the adjacent boundary layers. The bulge itself has wake-like characteristics in the mean flow, and much higher levels of Reynolds stress than in a two-dimensional (spanwise-invariant) reattaching flow. Well downstream, some Reynolds stresses ($\overline{u^2}$ and $\overline{uv}$) in the bulge fall below those in a standard boundary layer, as also observed by Castro & Epik (1998) in a two-dimensional coplanar flow. See also the paper of Song, de Graaff & Eaton (2000). Interestingly, there is a region of nearly constant shear stress beneath the bulge even though $\overline{uv}$ rises to much higher levels further out. The characteristics of this very persistent bulge have their origins in the bulge that is created in the separation bubble, and so accurate physical representation of these persistent features will quite likely depend upon the accurate physical representation of the separated flow; history effects are likely to be dominant.

The velocity measurements presented here were obtained using pulsed-wire anemometry, including measurements in the near-wall region by means of a special through-wall pulsed-wire probe. However, as the near-wall measurements have been presented in an earlier paper by Hardman & Hancock (2000), in an investigation of the near-wall layer, they are not discussed here in detail. Hardman and Hancock defined the near-wall layer as one in which the viscous no-slip condition is directly evident in the mean velocity profiles. The thickness of this viscous layer was about 0.05 bubble lengths (but expected to be dependent upon Reynolds number, of course.)

Further analysis of the near-wall layer, and in particular the Reynolds stresses and higher order moments, is given by Hancock (2005, 2007). Those papers explore the idea that each Reynolds stress has its own velocity scale. For the normal stresses tangential to the surface ($\overline{u^2}$ and $\overline{w^2}$), these scales are friction velocities, u'_τ and w'_τ, based on the root mean square (r.m.s.) of the respective wall shear stress fluctuation. Although the measurements given there were made in a two-dimensional coplanar flow, the scaling arguments are likely to apply more generally.

The overlying shear layer of the separation bubble entrains fluid from both above and below. The entrainment on the 'low-speed' side (i.e. from below) is provided by the reverse flow. This is why the reverse flow exists, but the presence of low pressure inside the earlier part of the bubble must assist in driving the reverse flow. If (in a two-dimensional flow) there was very little entrainment required by the shear layer the reattachment would be a long-way downstream (and at infinity in the absence of any entrainment mass flow or influence of pressure). In the case here some of the entrainment 'source' flow to the bulge is provided by the inward-going reverse flow from the adjacent side regions. Therefore, it is to be anticipated that the position of the attachment line should, all else constant, be further downstream than in a two-dimensional flow, as indeed is observed.

2. Flow rig and measurements techniques

As mentioned earlier and illustrated in figures 1 and 2, the separated flow was generated behind a vertical flat plate, made in two parts, mounted on the front of a horizontal, v-shaped splitter plate. The vertical plates were swept symmetrically with respect to the free-stream flow direction at angles of $\pm 10^\circ$. The sharp tips of the vertical plates were very slightly blunted in a grinding machine to give a closely controlled 'fence' height h_f of 10.0 mm above and beneath the splitter plate surfaces. The splitter plate was 3.0 mm in thickness and 1m in length at the sides. A flap, 0.5 m in length, at the rear of the plate was inclined slightly to make the bubbles above and below the splitter plate equal in size. The model was mounted on slender legs and spanned the whole width of the working section of wind tunnel 'B' of the wind tunnel laboratory, where the working section was 0.5 m high, 1.53 m wide and 2.5 m in length. The contraction and working section of this blow-down wind tunnel were rebuilt to give a working section of these dimensions specifically for this study in order to provide sufficient flow width in relation to bubble size, and thereby to keep end effects acceptably small. In this compromise, the bubble size was kept as large as possible so as to minimize the relative size of the pulsed-wire probes. A still greater flow width would have been at the expense of reduced working section height (to maintain flow speed and wind tunnel contraction ratio) and increased blockage – the ratio of h_f to working section half height. Improvements were made to the wide-angle diffuser between the fan and settling chamber, by means of an additional screen, to eliminate a separation (that was probably present prior to the changes) on a diffuser wall. Mean flow uniformity in the working section was better than $\pm 1\,\%$ and the background turbulence level (streamwise intensity, u'/U) was better than 0.3 %, though some of this measured level would have been electronic noise. Some measurements were also made behind an unswept fence of the same height, to provide a reference check on techniques and instrumentation, and behind a v-shaped fence of smaller height, though there is no need to report these here.

The flow width in relation to the bubble length at which the measurements were made was based on earlier measurements (Hancock & Castro 1993). They suggested

this ratio should be not less than about 4 for an unswept flow, the present flow being regarded, perhaps simplistically, as two such flows side-by-side, at least for moderate sweep angles. 'End effects' are largest near the surface, where residual lateral pressure gradients formed in the flow above exert their influence. The more recent study of Ciampoli & Hancock (2006), indicates (assuming the side-by-side equivalence) that the largest residual influence will have been in the mean wall shear stress, with an error of +2 %. The large eddy simulation by di Mare & Jones (2003), assuming spanwise invariance, and its good agreement with the present measurements regarded as spanwise invariant, namely those at $z = 380$ mm (see later), adds further support that the flow width was adequate. Surface flow visualization, interpreted in figure 2, showed the region of invariance to exist between $z \approx 300$ mm and $z \approx 480$ mm, and likewise on the opposite side. It is possible that some flow features may not have been fully free of end effects, but it is believed the associated discrepancy is small.

The free-stream reference velocity U_r in the upstream flow was 5.8 m s^{-1} throughout, giving a Reynolds number based on h_f of 3900. A low sweep angle ($\pm 10^\circ$) was used because, as will be seen and as already mentioned, even this resulted in a large effect in the central region. One drawback of the relatively weak crossflow was that special care was needed to measure the lateral velocity W with adequate accuracy. Also, although swept laminar boundary layers exhibit crossflow instability if the crossflow Reynolds number and sweep angle are large enough (Poll 1985), the present low sweep angle and Reynolds number means that crossflow instability is not expected to be present.

At separation the boundary layer was laminar, but the shear layer in this type of flow rapidly becomes turbulent through the Kelvin–Helmholz mechanism (see e.g. Yang & Voke 2001). Ruderich & Fernholz (1986) chose a Reynolds number of $h_f U_r/\nu$ of 14×10^3 as being sufficient for 'high'-Reynolds-number flow. Measurements by Hancock (2000) confirmed significant variation in $\overline{u^2}$ below this Reynolds number, the variation being larger as the Reynolds number was decreased, but argued that the other Reynolds stresses were less affected from the fact there was very little influence on mean velocity profiles, bubble length, surface pressure distribution and some turbulence parameters. The present flow is expected therefore to have had some residual Reynolds number dependence in some quantities; a higher Reynolds number would have required a larger wind tunnel if probe resolution was not to be degraded.

Instantaneous velocity and wall shear stress were measured by means of pulsed-wire anemometry, where the velocity was measured using one or other of two probes. One of these, the 'field' probe, was held from a five-component traversing mechanism mounted above the roof of the working section. The other, the 'through-wall' probe, was mounted in a plug supported by the splitter plate and controlled from the underside of this plate by means of a micrometre head allowing a position accuracy of better than 0.1 mm. Based on the work of Castro & Dianat (1990) and Schober, Hancock & Siller (1998), the pulsed wire was parallel to the surface and the sensor wires were perpendicular, the prongs passing through small holes in the surface of the plug which was flush with the plate surface. The probe had a maximum reach of 12 mm above the plate surface, complementing the minimum height of 5 mm at which the field probe could be held. The pulse and sensor wires of the probes were, respectively, 9 μm and 2.5 μm in diameter, and about 6 mm in length. The sensor wires were about 1.8 mm apart. The probes were driven by a Pela Flow Instruments unit, with a sensor current of 2 mA and a pulse duration of 4 μs. Results from the through-wall probe have already been reported (Hardman & Hancock 2000) in an analysis of the near-wall layer. Some of these measurements will be included here, but not with special discussion, therefore.

The velocity probe was calibrated against a Pitot-static reference probe, with the calibration fitted by a polynomial of the form $U = A(1/T) + C(1/T)^3$, where U is velocity, T is the time of flight and A and C are constants (see e.g. Castro & Haque 1987). U was in the range 0.2–7 m s^{-1}. The error in the streamwise and lateral velocities, U and W, were to within about ± 1 % and ± 2 % respectively as fractions of the reference velocity U_r. A number of probe configurations were tried before a final set was established. By using a dummy probe it was found that presence of the probe body, held vertically, had a measurable interference effect when it was near the reattachment position. To reduce this effect the probe body was made as slender as possible, and the fence height as large as possible without eliminating the side regions of spanwise invariance. The probe body diameter was 1.5 mm over the 85 mm nearest to the probe head, followed by diameters of 3 mm and 4 mm over the next two lengths of 85 mm. The influence on the reattachment length for the probes used was less than 3 %.

Pulsed-wire probes measure only one component of velocity (or wall shear stress), the component that is perpendicular to the plane defined by the pulsed and sensor wires. The probe therefore has to be rotated to several positions in order to measure more than one component and more than one higher order moment. Rotation about the vertical axis (the y-axis) to give W, $\overline{w^2}$, $\overline{uw}$, etc. was very straightforward. Rotation about the horizontal z-axis to give V, $\overline{v^2}$, $\overline{uv}$, etc. was also straightforward as the probe traversing mechanism provided pitch control, though it meant moving the probe traversing mechanism in a streamwise position and adjusting the height in order to keep the probe head at a fixed position. After some trials, this method was considered preferable to one using more than probe, held vertically, but with the probe head of each set at a fixed angle (e.g. 30°) from the vertical, as at least two other probes would have been required, and each would have required separate calibration.

The sensor wires were 'offset' at an angle of about 25° to the normal to the probe plane, to avoid the wake of one on the other during calibration (Castro & Haque 1987). Ideally, the yaw and pitch calibration of the probe is cosinal where, here, yaw and pitch refer to rotation of the probe head about the y and z axes, respectively. Castro & Cheun (1982) provide an analytical estimate of the errors arising from imperfect response, which particularly affects the Reynolds stresses and higher order moments. The yaw and pitch responses (the latter partly inferred from the probe's construction) exceeded $\pm 80°$. The parameter ε of Castro and Cheun was in the range $0 < \varepsilon < 0.03$, implying a much closer cosinal response than that considered typical in that paper. The implied error in mean velocity is around 1.5 % of the local mean velocity. Errors in $\overline{u^2}$ are estimated to be within about ± 5 % while the errors in $\overline{v^2}$, $\overline{w^2}$ and $\overline{uv}$ are within about ± 10 %. The vertical velocity v could not be measured below $y = 5$ mm. Velocity gradient effects are only significant near the surface, when $u'_\tau y/\nu$ is 10 or less (Hancock 2005), and are not relevant to the results presented here.

The wall shear stress probe comprised two sensor wires of 2.5 μm diamater, about 1 mm apart and 2.3 mm length, and a 5 μm diameter pulsed wire, 3.3 mm in length, all held about 50 μm above the surface. The probe was calibrated against a Preston tube (using the calibration of Patel 1965) in a standard zero-pressure-gradient turbulent boundary layer on the floor of the wind tunnel, with the calibration measurements fitted to a polynomial of the form $\tau_w = A + B\overline{1/T} + C\overline{(1/T)^2} + D\overline{(1/T)^3}$, where T is the time of flight of each sample and the overbars denote time averages, the flow being turbulent. A, B, C and D are calibration constants also obtained using the method of least squares. Once calibrated, the probe is in effect an absolute device

for measuring wall shear stress. The accuracy of the calibration for the mean shear stress τ_W is expected to be within about $\pm 3\,\%$. The cosinal response of the wall shear stress probe exceeded $\pm 85^\circ$; the associated errors are negligible. It is important (for the shear stress probe) for the quadratic and cubic terms to be calculated correctly (rather than using $\overline{1/T}^2$ and $\overline{1/T}^3$ which gives an error of about 4 %); there is no difficulty in doing this.

The finite length l of the wires (of the shear stress probe) results in a spatial averaging of the structures detected by the probe, having a significant effect on the mean square of the fluctuating velocity. The non-dimensional length lu'_τ/ν was in the range 18–30. Effects of spatial averaging are discussed by Castro, Dianat & Bradbury (1987) and Dengel, Fernholz & Hess (1986) for boundary layers and by Hancock (1999), where the last concludes that beneath separated flows spatial averaging by the present probe should have amounted to not more than about an 8 % reduction in τ' at $lu'_\tau/\nu = 30$, where τ' is the r.m.s. of the wall shear stress fluctuation. This is substantially less than it would be for a boundary layer because large-scale motions generated in the overlying shear layer play a much larger role in the near-wall motions (Adams & Johnston 1988; Fernholz 1994; Na & Moin 1998). The effect on the mean wall shear stress was negligible. Based on the height s of the wires above the surface (nominally 0.05 mm) the non-dimensional height of the wires su'_τ/ν did not exceed 0.7. As discussed by Hancock (2005, 2007), the viscous sublayer for the fluctuations is not linear, even at this small distance. Nevertheless, the error in τ' will not have exceeded 10 %, at most.

The pulsed-wire probe and flow-visualization were used to measure the location of the attachment line. In a two-dimensional coplanar flow this is straightforward in that it corresponds to the position at which the shear stress vector is parallel to the (known) separation line. In less special circumstances it is necessary to measure the shear stress vector direction and locate the line along which the vectors converge to form the attachment line (the shear stress perpendicular to the attachment line is zero, and non-zero along it, except at singularities). However, as there were only relatively few lateral measurement stations, oil-flow visualization and the ink-dot method of Langston & Boyle (1982) were the primary means of locating the loci of the limiting streamlines. The pulsed-wire measurements were in good agreement with streamline direction so obtained.

As noted earlier, both the velocity probe and the wall shear stress probe measure only one component of velocity or shear stress. It is therefore necessary to rotate these probes to obtain orthogonal components and associated cross products. For the mean velocities U and W:

$$U_{\theta_i} = U\,\cos(\theta_i) + W\,\sin(\theta_i), \tag{2.1}$$

where U_{θ_i} is the mean velocity measured by the probe at some angle θ_i to a reference direction. By subtracting the instantaneous from the mean it is straightforward to show that the mean square velocity fluctuation $\overline{u^2}|_{\theta_i}$, measured by the probe at angle θ_i to the reference direction, is given by

$$\overline{u^2}|_{\theta_i} = \overline{u^2}\cos^2(\theta_i) + \overline{uw}\sin(2\theta_i) + \overline{w^2}\sin^2(\theta_i), \tag{2.2}$$

where $\overline{u^2}$, $\overline{uw}$ and $\overline{w^2}$ are Reynolds stresses, obtained by a least squares fitting routine, as were U and W. Typically, five angles of pitch (for $u \sim v$ products) and five angles of yaw (for $u \sim w$ products) were employed at intervals of 20° from zero so as to provide redundancy of measurement, which is desirable in pulsed-wire anemometry as

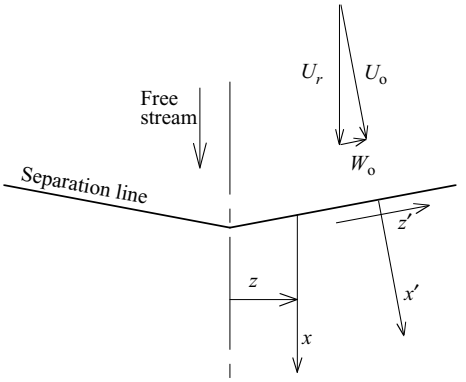

FIGURE 3. Coordinate axes.

it provides a self-consistency check on the angle sensitivity. The angles were selected so that the flow direction onto the probe was close to optimal with respect to the response cone. Mean flow directions in excess of $\pm 45^\circ$ with respect to the probe flow axis were excluded, which meant that sometimes only four of the five orientations were used. The uncertainty in $\overline{u^2}|_{\theta_i}$ against that from the fitting routine was about $\pm 5\,\%$. The corresponding equation for the third-order moments involves four terms on the right-hand side, requiring four or more distinct angles. These moments are not given here, as additional redundancy would have been preferred.

A similar expression to that of (2.1) arises for the mean wall shear stresses, τ_x and τ_z:

$$\tau_{\theta_i} = \tau_x \cos(\theta_i) + \tau_z \sin(\theta_i). \tag{2.3}$$

And for the mean square of the measured wall shear stress fluctuation $\overline{\tau'^2}|_{\theta_i}$, the relationship is

$$\overline{\tau'^2}|_{\theta_i} = \overline{\tau'^2_x} \cos^2(\theta_i) + \overline{\tau'_x \tau'_z} \sin(2\theta_i) + \overline{\tau'^2_z} \sin^2(\theta_i), \tag{2.4}$$

where $\overline{\tau'^2_x}$ and $\overline{\tau'^2_z}$ are the mean squares of the fluctuating wall shear stresses in the x and z directions, respectively, and where $\overline{\tau'_x \tau'_z}$ represents the correlation of the wall stress fluctuations. Again, a least-squares fitting routine was used, though generally with fewer probe orientation angles necessary. Fitting errors were negligible for the fluctuating wall shear stress measurements,

Each measurement of the left-hand sides of (2.1)–(2.4) was obtained from 5000 samples over 170 s, equivalent to in excess of 6000 time scales based on the free-stream velocity and bubble length (X_A). This was sufficient to provide smooth fits to to these equations and smooth profiles of mean and second-order moments; in effect the terms on the right-hand sides of (2.1)–(2.4) were obtained from at least 20 000 samples.

Measurements were made in planes at seven lateral positions z, namely -40, 0, 40, 80, 120, 200 and 380 mm, where z is defined in figure 3, or, in terms of h_f, $z/h_f = -4$, 0, 4, 8, 12, 20 and 38, all but the last being where lateral variations were expected to be significant, as inferred from the surface streamlines. All locations coincided with a system of slots and instrumentation plugs in the splitter plate surface, allowing the wall shear-stress and through-wall probes to be placed at any streamwise position x from $4h_f$ to $40h_f$. The plane at $z = -40$ mm, by comparison with that at $z = +40$ mm, was used only in preliminary measurements to confirm symmetry in the flow.

z/h_f	0	4	8	12	20	38
X/h_f	25.9	24.5	23.5	23	22	21
X/X_0	1	0.95	0.91	0.89	0.85	0.81

TABLE 1. Distance to the attachment streamline.

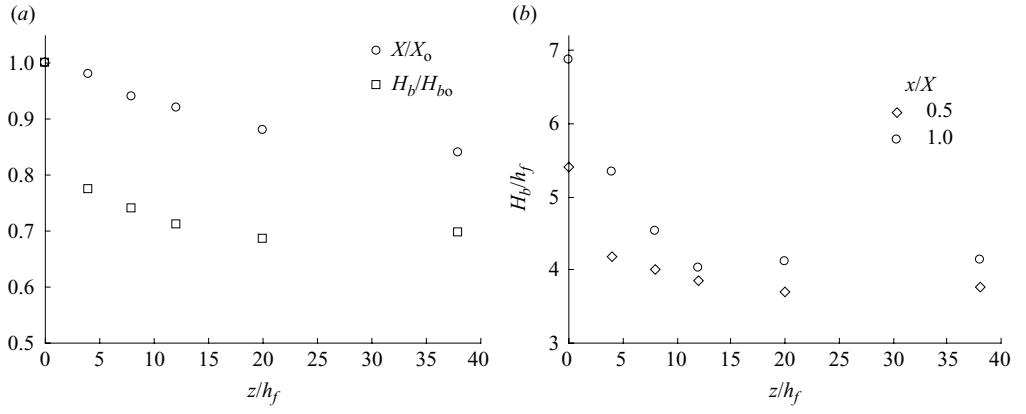

FIGURE 4. Bubble height and length.

3. Results and discussion

3.1. *Mean flow*

The coordinate axis system used for presenting the results is given in figure 3, and unless otherwise stated 'wind tunnel axes' x–z are used throughout. y is perpendicular from the splitter-plate surface, and zero on it.

Measurements were made at five streamwise stations, nominally at $x/X = 0.25$, 0.5, 0.75, 1 and 1.25, at six lateral positions of $z/h_f = 0$, 4, 8, 12, 20 and 38, where $x/X = 1$ is the position of the attachment line at each lateral position, as measured by the pulsed-wire wall shear stress probe. X is given in table 1, normalized by h_f and by X on the centreline, X_0, and in figure 4(a), where it can be seen that in the spanwise-invariant region it is 19 % less than on the centreline, where it is a maximum. As will be seen, W, $\overline{uw}$ and τ_z are all zero on $z = 0$, within the uncertainty of measurement. The surface flow visualization, figure 2, also showed the flow to be closely symmetrical.

Figure 4 also summarizes the shape of the bubble in terms of its height H_b defined in terms of the height at which U is 0.95 of the local maximum. Figure 4(b) shows the height at two streamwise stations, $x/X = 0.5$ and 1.0, from which it can be seen that the variation in height is larger at the second station. The variation in height at the mid-position is also shown in figure 4(a), but as a fraction of the height on the centreline H_{b0}. Clearly, the variation in height is notably larger than the variation in the distance to attachment, though qualitatively this is not surprising in that there has to be an 'outflow' from the rear of the bubble, as described earlier in § 1 and illustrated in figure 1. Figure 4 shows little variation in bubble height with z, beyond $z/h_f = 20$.

Figure 5 shows the pressure coefficient, defined as $C_p = (p - p_r)/(1/2)\rho U_r^2$, on the splitter-plate surface, where p_r is the static pressure at the reference station. As

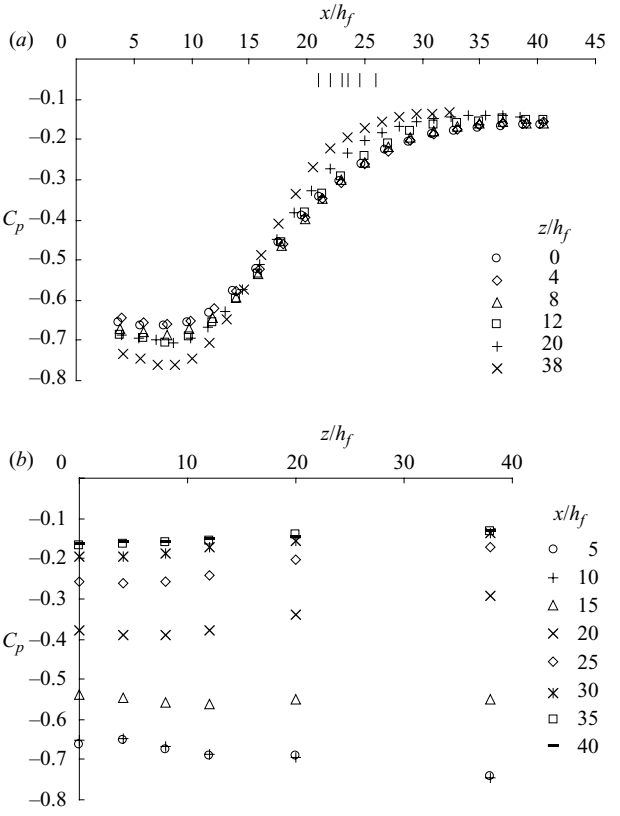

FIGURE 5. Variation of pressure coefficient with (*a*) x/h_f and (*b*) z/h_f. The vertical lines in (*a*) show X/h_f for the six lateral stations.

expected, the pressure is higher on and near $z=0$ than it is at $z/h_f=38$. However, this persists for only part of the flow. Beyond about half a bubble length downstream the pressure is lower on and near $z=0$. The limiting streamlines on the splitter as inferred from both surface oil flow and the ink-dot method are shown in figure 2. A line of secondary separation will have existed, as given by McCluskey, Hancock & Castro (1991), but was not picked out in the interpretation of the surface-flow patterns obtained here. Their work showed the secondary separation lines in the spanwise-invariant regions merging into foci singularities, one each side of the centreline and no secondary separation on the centreline. Figure 6 shows the mean wall shear stress coefficients, C_{fx} and C_{fz}, as obtained from the wall shear stress probe, where the wall shear stresses are normalized by $(1/2)\rho U_r^2$. C_{fz} is satisfyingly close to zero on $z=0$, though the scatter from one point to the next is an indication of the uncertainty in C_{fz}. (C_{fz} is obtained by difference, and errors can compound rather than cancel.) The streamwise wall shear stresses are generally lower in the central region than in the spanwise invariant region, as might be anticipated in terms of the greater height of the bubble, except for $z=0$. Extrapolation of these profiles to smaller x indicates secondary separation except on the centreline. Figure 7 shows the negative peak magnitudes of C_{fx} and C_{fz}. Ideally, given the change in C_{fx} between $z/h_f=20$ and $z/h_f=38$, there would have been another station between these two positions; in the absence of one it is supposed that C_{fx} continues to increase fairly steeply outside

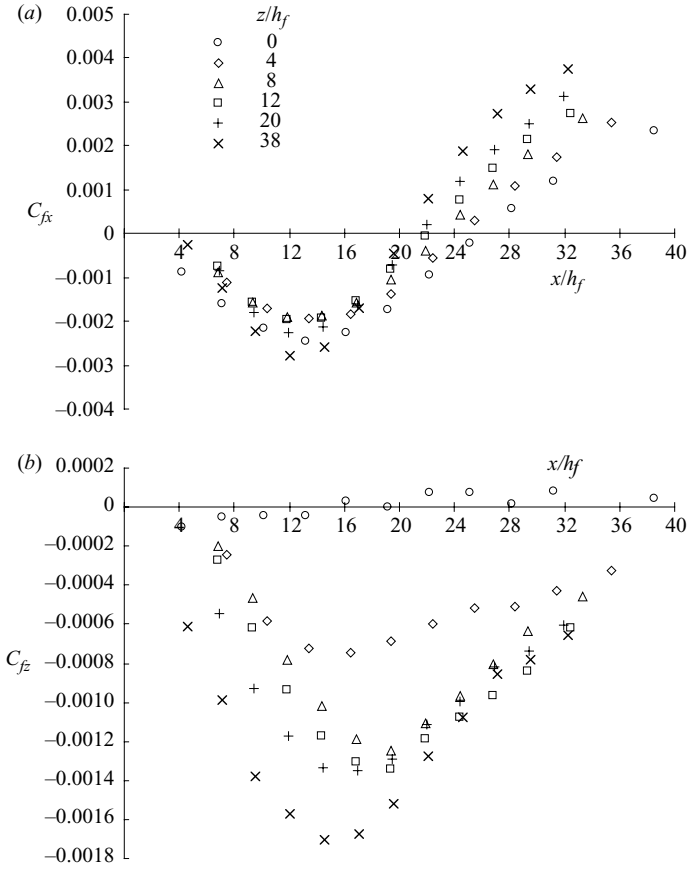

FIGURE 6. Mean shear stress coefficients C_{fx} and C_{fz}.

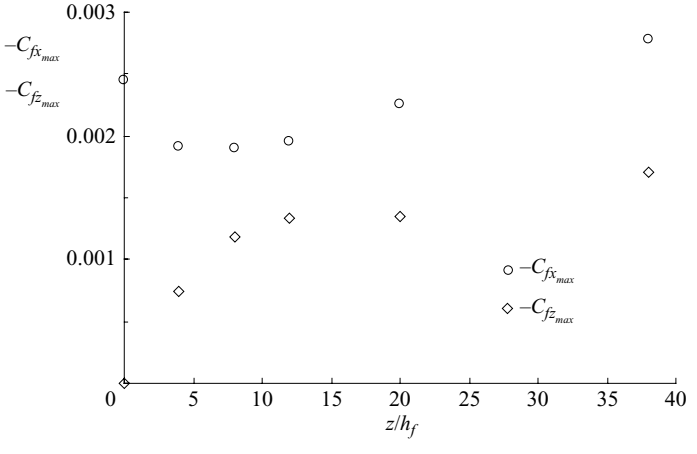

FIGURE 7. Variation of negative peak magnitudes of C_{fx} and $C_{fz}$with z/h_f.

$z/h_f = 20$. A plausible curve can be drawn through the points for C_{fx} and, with an allowance for the uncertainty just mentioned, a plausible curve can be drawn through the points for C_{fz}, such that their gradients are zero at $z/h_f = 38$.

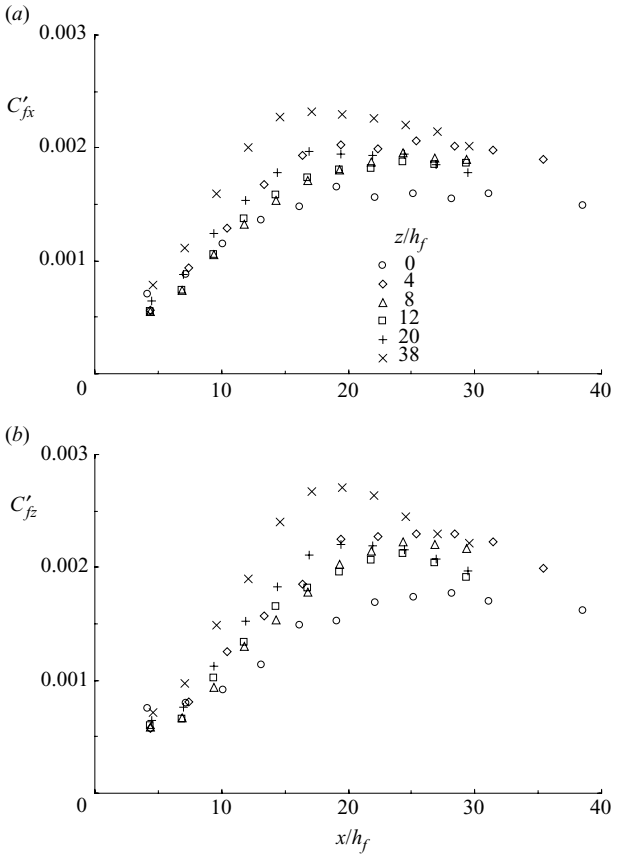

FIGURE 8. Coefficients of r.m.s of fluctuating shear stress, C'_{fx} and C'_{fz}.

Although a measure of the turbulence rather than the mean flow, it is convenient at this point to introduce the coefficients for the fluctuation in wall shear stress, C'_{fx} and C'_{fz}, defined as the r.m.s. of τ'_x and τ'_z, normalized by $(\frac{1}{2})\rho U^2_{ref}$. These are shown in figure 8, where they are seen to be very comparable in magnitude, suggesting the fluctuation magnitudes at any particular location are only weakly dependent on direction. Interestingly, C'_{fx} and C'_{fz} are smallest on the centreline, unlike C_{fx}, and are consistent with the idea that shear-stress fluctuations are driven primarily by the large-scale structures in the outer flow, which are furthest from the surface at this z location. By way of example, it is obvious that the mean and fluctuating stresses are not linked as C_{fz} is zero on the centreline.

Profiles of the mean velocities, U, V, W are shown in figure 9, for all x and z stations. Notice that the profiles of W on $z=0$ are also satisfyingly close to zero, a necessary condition for flow symmetry, though no such assumption was made in obtaining W, and neither was it in obtaining C_{fz}. The U profiles show the greater height of the bubble near the centreline. Also, this greater height is seen to cover a wider lateral extent at each successive x station. At the first station ($x/X \approx 0.25$) all but the profile on $z=0$ are close together, whereas at the last station ($x/X \approx 1.25$) at least three of the lateral stations show a clear difference from those at $z/h_f = 20$ and 38 – the region of influence on U gets wider. There is a curious contrast with the profiles of W. At the first station all the profiles differ, while at the last station

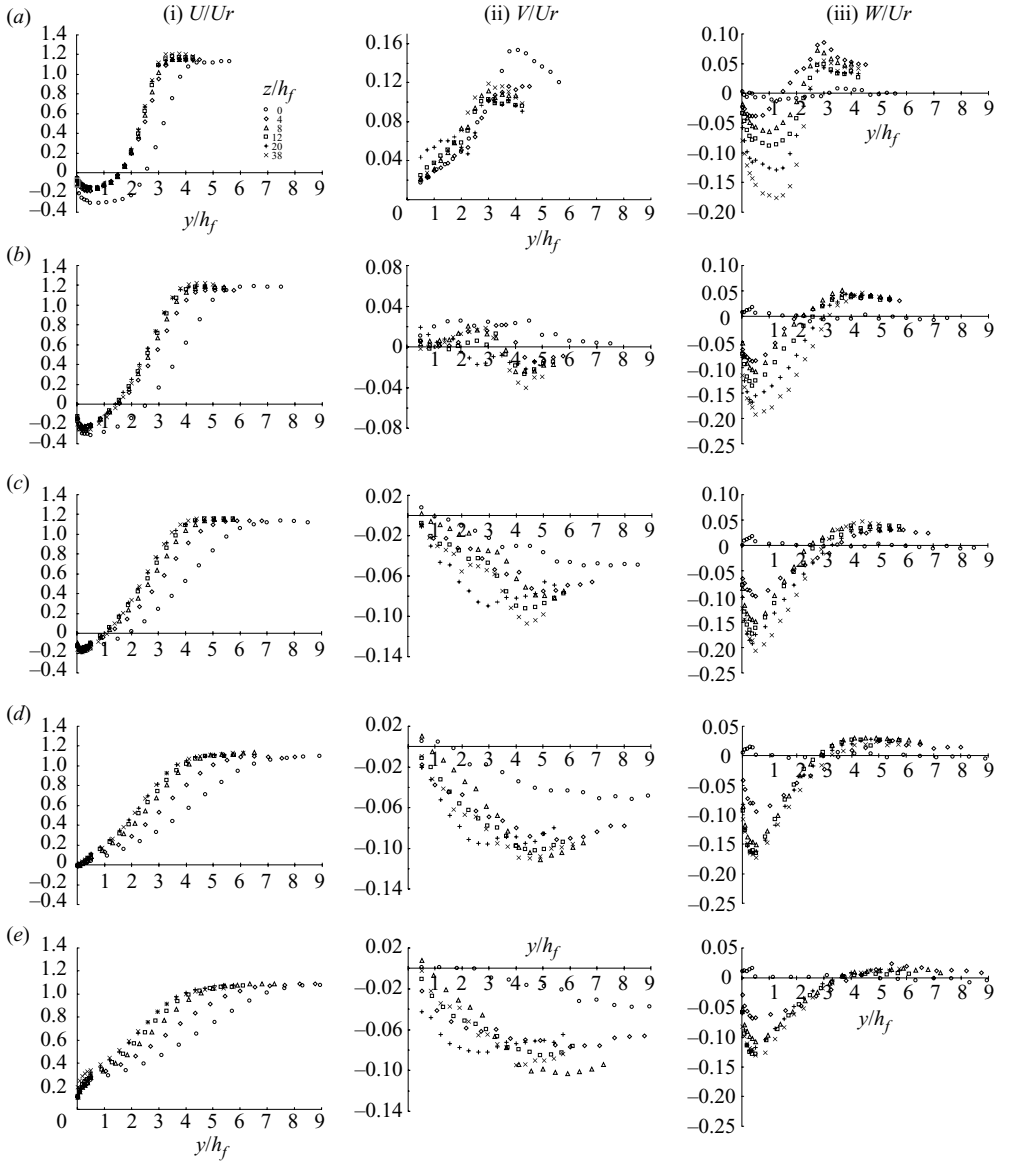

FIGURE 9. Mean velocity profiles, U, V and W, at the five streamwise stations. (*a*) $x/X = 0.25$; (*b*) 0.5; (*c*) 0.75; (*d*) 1.0; (*e*) 1.25.

the outer four profiles fall close to each other. Thus the region over which W is influenced gets *narrower* with each successive station. The variation of the inward lateral mean velocity W (< 0) is summarized in figure 10 in terms of the maximum negative velocity.

These profiles in figure 9 show, as expected, that U is larger than upstream free-stream speed U_r above the bubble, where W is positive, rather than negative. There is virtually no variation in the maximum U with z, even though a thicker bubble might be expected to give a larger U. The fact that W is positive near and above the bubble edge is, perhaps surprising at first sight. However, it is straightforwardly explained by the inviscid acceleration of the component of velocity in a direction normal to the

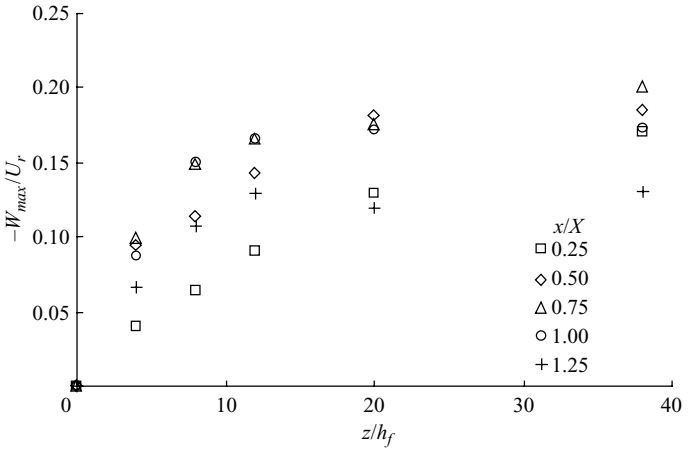

FIGURE 10. Variation of $-W_{max}/U_r$ with z/h_f.

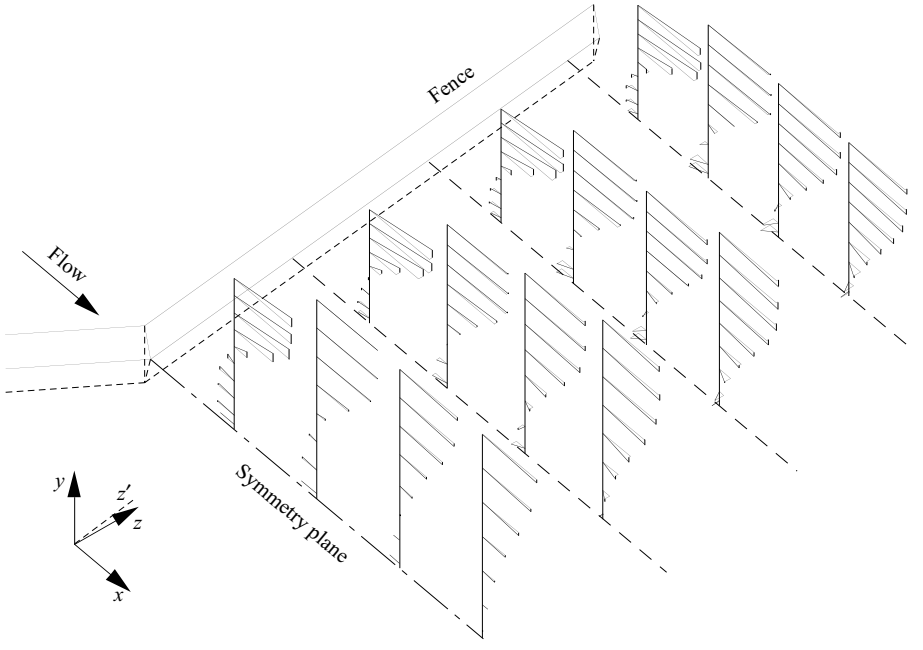

FIGURE 11. Mean velocity vectors at four streamwise and four lateral stations. The vectors are to scale, as are their locations.

fence. This velocity has a component contributing to W, where this contribution is larger near the front of the bubble. Nearer the surface W is negative, providing the expected inflow towards the central region.

The profiles of V are broadly close together, except that on $z = 0$, which becomes progressively more positive with downstream distance relative to the others at the same streamwise location. The last feature is consistent with the increased height of the bubble. To aid visualization of the mean velocity field, figure 11 shows a vector diagram over a region covered by the first four x- and z-wise stations.

A feature that was not anticipated is the larger reverse-flow velocity seen in U at $x/X = 0.25$ and less so at $x/X = 0.5$, near the centre (figures 9i*a* and 9i*b*). In a two-dimensional coplanar flow the reverse flow is driven by the entrainment requirement of the overlying free shear layer, aided by a favourable pressure gradient. Here, the favourable pressure gradient is less strong in the central region, as can be seen from figure 5, and entrainment into the shear layer is also provided by the lateral inflow from the sides (as seen in the profiles of W). One possibly linked fact is that there is no secondary separation on $z = 0$, the surface limiting streamlines forming into two contra-rotating foci singularities of separation either side of the centreline, as outlined earlier. Certainly, the sense of rotation of these foci is consistent with an induced increase in negative U.

The mean velocities U and W can be re-expressed with respect to axes aligned with the angle of the fence, ('fence' axes, rather than the 'tunnel' axes). If a prime denotes these velocities then

$$U' = U\cos(\theta) + W\sin(\theta) \qquad \text{and} \qquad W' = W\cos(\theta) - U\sin(\theta),$$

where θ denotes the sweep angle, the angle between z and z' (figure 3). Because the sweep angle is small and W is also relatively small, profiles of U' are very close in shape to the profiles of U, and so are not presented. However, the profiles of W' are very different from those of W. Figure 12 shows profiles of W' normalised by $W_0 = U_r\sin(\theta)$, together with profiles of flow direction, $\tan^{-1}(W/U)$ – where W and U are the velocities in wind tunnel axes. The x'–z' axis system is a natural one behind a swept separation line where, by definition, profiles would be invariant with lateral position in a spanwise-invariant flow, but is not a particularly natural one in the current flow, or not obviously so. Nevertheless, some notable observations emerge that are not seen from the earlier profiles, and are set out next. Note, well above the surface W'/Wo approaches -1, since W approaches zero and U approaches U_r (if we ignore the small effect of wind tunnel blockage).

At the first x station ($\sim$0.25) the profile for $z/h_f = 38$ is seen to have a dip in magnitude near y/h_f of about 2.7. The profile at $z/h_f = 20$ shows a similar feature, and the profiles at $z/h_f = 12$ and 8 show a clear development of the trend, as do the profiles at $z/h_f = 4$, and $z/h_f = 0$. At first, this dip, particularly at the outer-most station seems rather odd. Why should the velocity parallel to the separation line in a spanwise-invariant flow first decrease and then increase as the surface is approached? Precisely the same sort of behaviour is very clearly present in the direct numerical simulation of Kaltenbach & Janke (2000), though with little comment. The adjacent part of figure 12 shows the corresponding flow-direction profiles. The flow direction on $z = 0$, taking it to be a plane of symmetry, has to be either zero or –180°. In each case, except for this profile, the flow direction is very nearly zero above $y/h_f = 2.3$ but, as can be seen from figure 9i(a), the U-component velocity has already decreased appreciably at this height. Beneath this height, the flow direction changes rapidly. By rewriting the above equation for W' as

$$\frac{W'}{W_0} = \frac{W}{U_{ref}}\frac{\cos(\theta)}{\sin(\theta)} - \frac{U}{U_{ref}}$$

it can be seen that if W is zero then

$$\frac{W'}{W_0} = -\frac{U}{U_{ref}},$$

and the profile of W' is like that of U; W' will decrease as U decreases. If, further in, W becomes negative, the magnitude of W' must increase, and the profile of W' will no longer follow that of U. Thus, in summary, the flow direction in the outer part

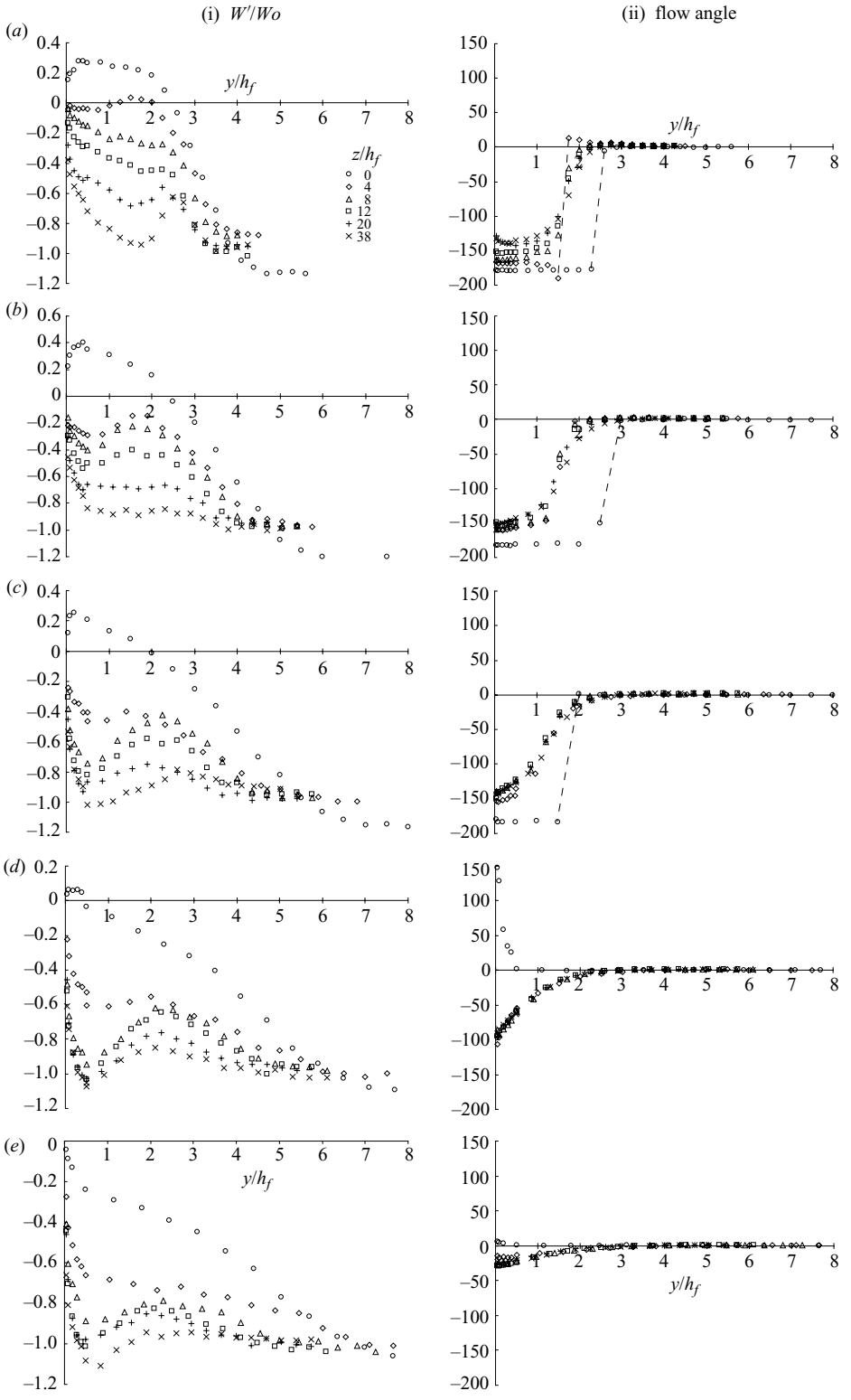

FIGURE 12. Profiles of W'/W_0 and flow angle. (*a*) $x/X = 0.25$; (*b*) 0.5; (*c*) 0.75; (*d*) 1.0; (*e*) 1.25.

of the shear layer remains very near zero. As a consequence, both W' and $U(\approx U')$ decrease in proportion. But, further in, the flow direction changes rapidly, with the result that W' increases in magnitude (above what it would be were the flow direction to remain zero). The marked change in gradient in the W' profiles is therefore linked to the rapid change in flow direction that takes place within the shear layer. It seems that, in effect, the outer side of the shear layer resists a crossflow that exists nearer the surface.

The flow-direction profiles at the other four streamwise stations (figure 12ii*b–e*) also show markedly similar sets of profiles at all except the central lateral station. There is no obvious reason why the flow direction profiles should exhibit similarity, so it is taken as fortuitous. There is though, one noticeable feature, again taken as fortuitous, that the flow direction is about zero above $y/h_f = 2.3$, as at the first station. This height does not appear to relate to a particular feature in the profile of U (or U'). It does, however, relate to a marked change in the profiles of W'. Below this height, in nearly all profiles, W' either increases in magnitude or does not decrease as rapidly as it was decreasing (above this height). The earlier measurements of Hancock & McCluskey (1996) behind a fence swept at a larger angle of 25° also showed a near-streamwise flow direction in the outer part of the shear layer, though W' levelled out rather than increased with decreasing height. As to a mechanism for this increase in W' seen at $x/X = 0.25$, it is supposed that it is associated with the reverse flow transporting 'large' W' from nearer reattachment, where, as anticipated, W' is fairly constant (except close the surface, where it must go to zero). The reverse flow (at the spanwise-invariant station) transports the large W', except further from the surface where the shear layer has greater influence, maintaining flow direction even where the velocity magnitude is reduced, the reduced magnitude implying a reduced W' from what it is in the free stream, as explained earlier. On top of this, there are the effects of the gradients $\partial\overline{uw}/\partial x$ and $\partial\overline{vw}/\partial y$, which may be significant. The latter is likely to be larger than the former on the basis that the bubble height is significantly smaller than its length. If these gradients are negligible then W' behaves as a passive contaminant, constant along streamlines in the y–x' plane, outside the influence of viscous diffusion. That the flow direction remains constant in the outer part of the shear layer is intriguing in itself, though the mechanism by which this happens is not clear. The reverse flow becomes the flow that is entrained into the shear layer but, in the earlier part of the bubble at least, this reverse flow appears to be a largely separate entity from the overlying shear layer.

The last feature of the mean flow to consider for the present is the thickness and position of the free shear layer. The gradient thickness is defined as $L = \Delta U/(\partial U/\partial y)_{max}$, where ΔU is the difference between the maximum and minimum in U, namely $U_{max} - U_{min}$, except downstream of attachment, where ΔU is $U_{max} - U_i$. Upstream of attachment $U_{max} - U_{min}$ is a sensible velocity difference to take as a scale of the shear layer, sensible in that to a first approximation it ignores the near-wall viscous layer. Downstream of attachment U_{min} is zero because U is everywhere positive. U_i is the velocity at the outer edge of the wall viscous layer, and provides a more sensible velocity from which to form ΔU, than one based on U_{min}. U_i has been judged from where the velocity profiles make a clear change in gradient near the surface. A height y_c for the centre of the shear layer can be defined as the point at which the velocity is equal to $0.67\Delta U + U_{min}$, which corresponds to the centre of a plane mixing layer (see e.g. Castro & Bradshaw 1976), where downstream of attachment U_{min} is replaced by U_i. Although the quantitative evaluation of U_i is of course approximate, a more exacting definition would not alter the inferences drawn here. Profiles of L/X and y_c/X are given in figure 13, where the greater height of the

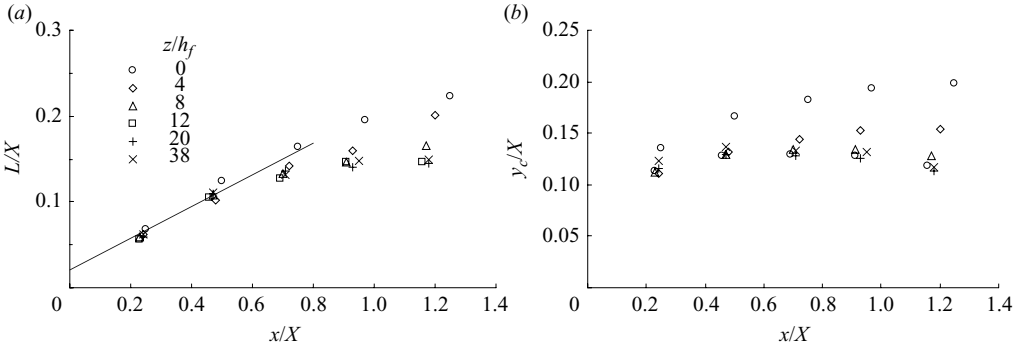

FIGURE 13. Variation of gradient thickness L and shear-layer centreline y_c with x/X. Line in (*a*) is from Hancock (2000).

bubble near the centre can be seen in figure 13(*b*). Away from centreline the growth in L is as observed in two-dimensional flows (e.g. Castro & Haque 1987; Jaroch & Fernholz 1989; Hancock 2000), with a marked decrease in the growth rate after roughly $0.6X$. Near the centre the growth rate remains much more nearly constant. Here, the structures in the bulge are further from the wall (figure 13*b*) and so, it is surmised, contribute less to the reverse flow.

3.2. *Reynolds stresses*

Four Reynolds stresses, namely $\overline{u^2}$, $\overline{w^2}$, $\overline{v^2}$ and $-\overline{uv}$ are given in figure 14 at the same streamwise and lateral stations as the mean velocity profiles. $\overline{u^2}$ and $\overline{w^2}$ are plotted to the same scale as each other, as are $\overline{v^2}$ and $-\overline{uv}$, while $\overline{uw}$, which is much smaller in magnitude, is given separately in figure 15. $\overline{w^2}$, though smaller than $\overline{u^2}$, has profiles that are comparable in shape, except at $x/X = 1.25$, where there is very little rise with distance from the surface compared with that seen in $\overline{u^2}$. Generally, the peak in a profile of $\overline{u^2}$ is further from the surface than is the peak in the corresponding profile of $\overline{w^2}$. Broadly, near the centre (i.e. near $z = 0$), the profiles reach higher levels and the profile outer edges are further from the surface than they are at stations further from the centre. The greater distance of the profile edges is as to be expected from the mean flow, of course. Another notable feature is that, at each x/X, the profiles of $\overline{u^2}$ converge near the surface to very comparable levels, and the same is seen in the $\overline{w^2}$. Moreover, at each x/X, the levels of $\overline{u^2}$ and $\overline{w^2}$ near the surface are close to each other even though the peak levels further out are significantly different. Indeed, at the last streamwise station, $\overline{w^2}$ is a little larger than $\overline{u^2}$. Turning to $-\overline{uv}$, the profiles of this shear stress are quite close in shape to those of $\overline{u^2}$. The profiles of $\overline{v^2}$ also show greater bubble height near the centre, but are more varied than the other Reynolds stresses.

As already noted, $\overline{uw}$ is much smaller in magnitude than other stresses, as might be anticipated for moderate three-dimensionality. Satisfyingly, $\overline{uw}$ is close to zero on $z = 0$, all except for a small number of points, which is attributed to statistical error. The negative $\overline{uw}$ seen at $z/h_f = 4$ for the last three stations stands out from the rest, but is probably genuine. At this station the lateral slope of the overlying shear layer, as inferred from the variation in bubble height with z, is large. If, locally, the shear layer behaves as a two-dimensional shear layer but at an angle ϕ to the surface (in the y–z plane), then $\overline{uw} \sim \overline{uv'}\sin(\phi)$, where v' is the fluctuation perpendicular to the shear layer. From figure 4(*b*), ϕ is roughly 11°; with $-\overline{uv'}$ typically $\sim 0.02U_r^2$, $\overline{uw}$ is about -0.004, which is very comparable with that seen in figure 15. The only

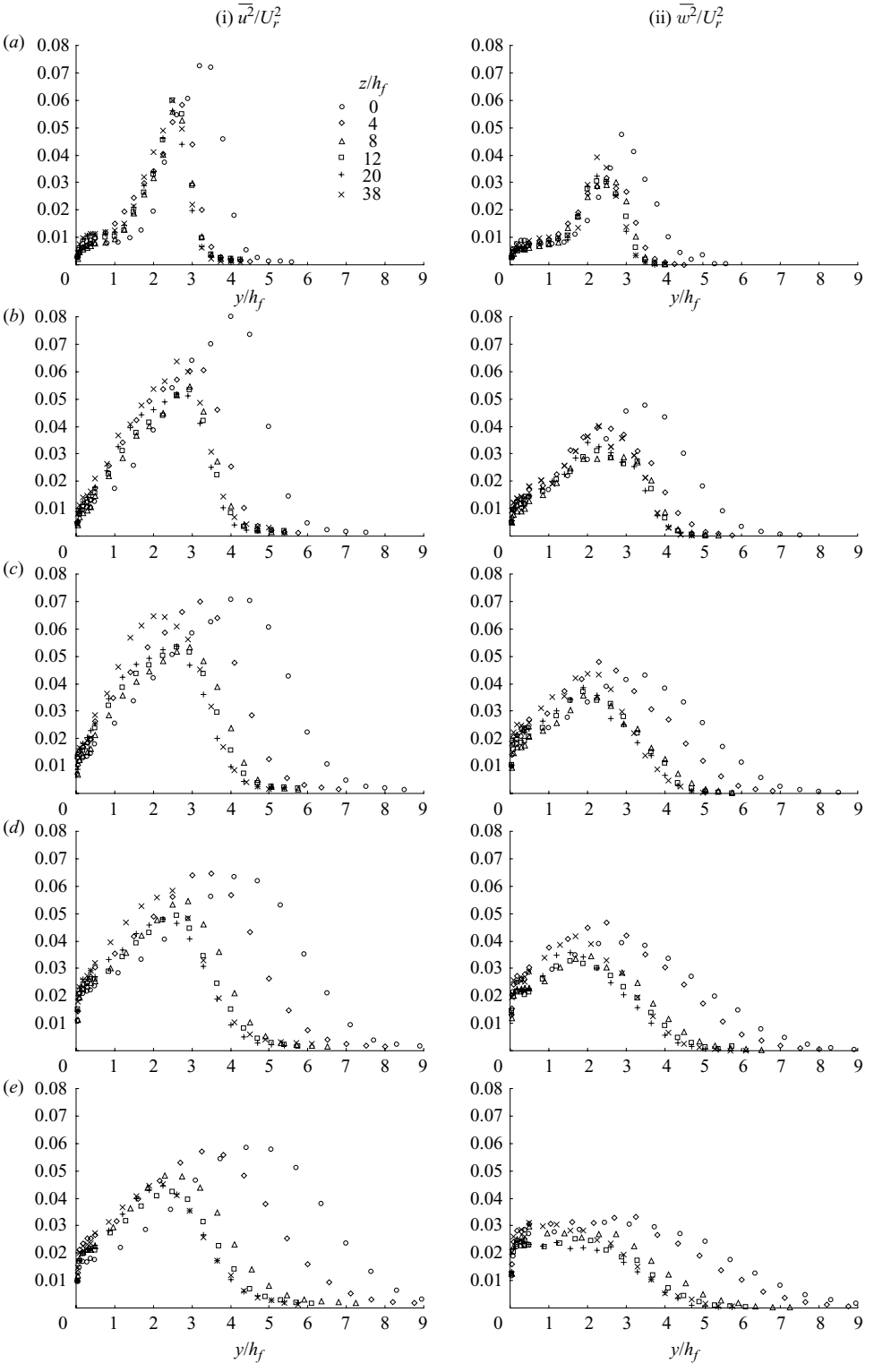

FIGURE 14. (Part i) Reynolds stresses, $\overline{u^2}$ and $\overline{w^2}$, at the five streamwise stations, normalized by U_r^2. (*a*) $x/X = 0.25$; (*b*) 0.5; (*c*) 0.75; (*d*) 1.0; (*e*) 1.25. (Part ii) Reynolds stresses, $\overline{v^2}$ and $\overline{uv}$. Symbols are as in Part i.

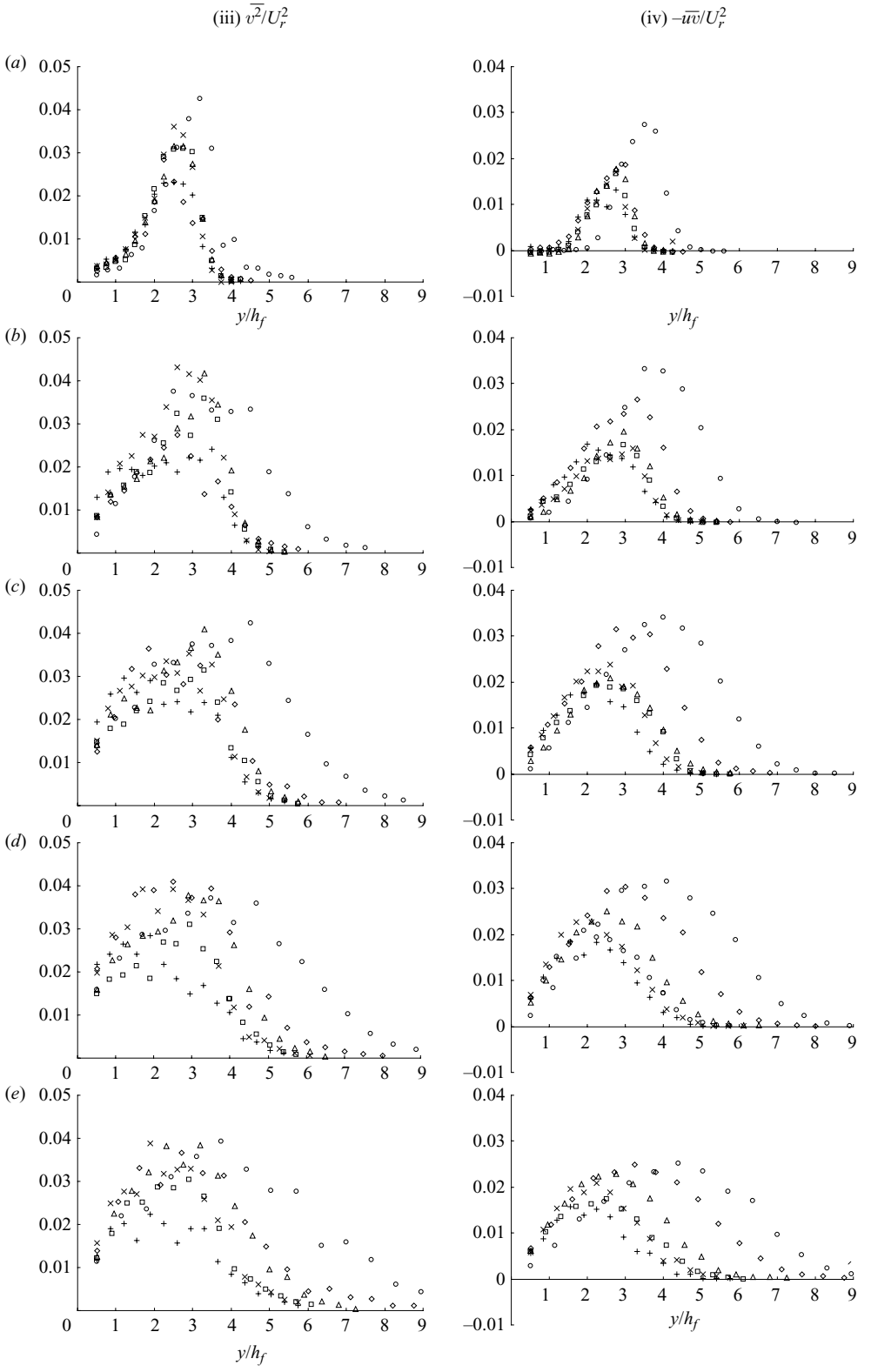

FIGURE 14. Continued.

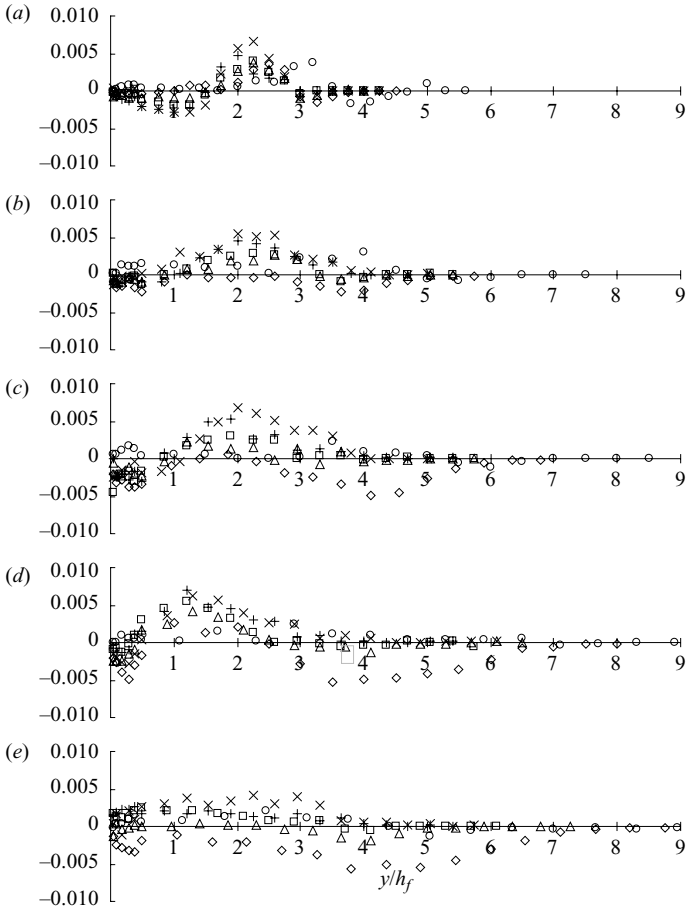

FIGURE 15. Reynolds stress $\overline{uw}$. (*a*) $x/X = 0.25$; (*b*) 0.5; (*c*) 0.75; (*d*) 1.0; (*e*) 1.25. Symbols as in figure 14.

other point to note here regarding the profiles in this figure, is the consistent small positive peak at the first four stations. This peak moves inwards slightly with each successive station, and is perhaps linked to the slight inward movement in the peak of $\overline{w^2}$.

Peak levels of Reynolds stresses are given in figure 16, as functions of z, and figure 17 gives peak levels of the turbulence kinetic energy. The general trend of these profiles is to show a decrease in the level of the Reynolds stresses as z/h_f decreases from $z/h_f = 38$ to where they are a minimum at about $z/h_f = 20$, with the exception of $\overline{w^2}$ which shows a minimum further in at about $z/h_f = 10$, over the length of the bubble. Nearer to centreline the levels rise. The decrease in turbulence levels is to be expected from the negative spanwise stretching, i.e. negative $\partial W/\partial z$, tending to decrease turbulence intensities. The rise in turbulence levels is therefore particularly interesting. The x-direction wall shear stress (figure 6*a*) also shows a decrease and a subsequent increase, with decreasing z. Both wall shear stress fluctuations show, in figure 8, a decrease in their r.m.s. levels with decreasing z until $z/h_f = 12$ and 8, where they differ little. Further in, both r.m.s. levels first rise consistently, before falling to the lower levels seen on $z = 0$.

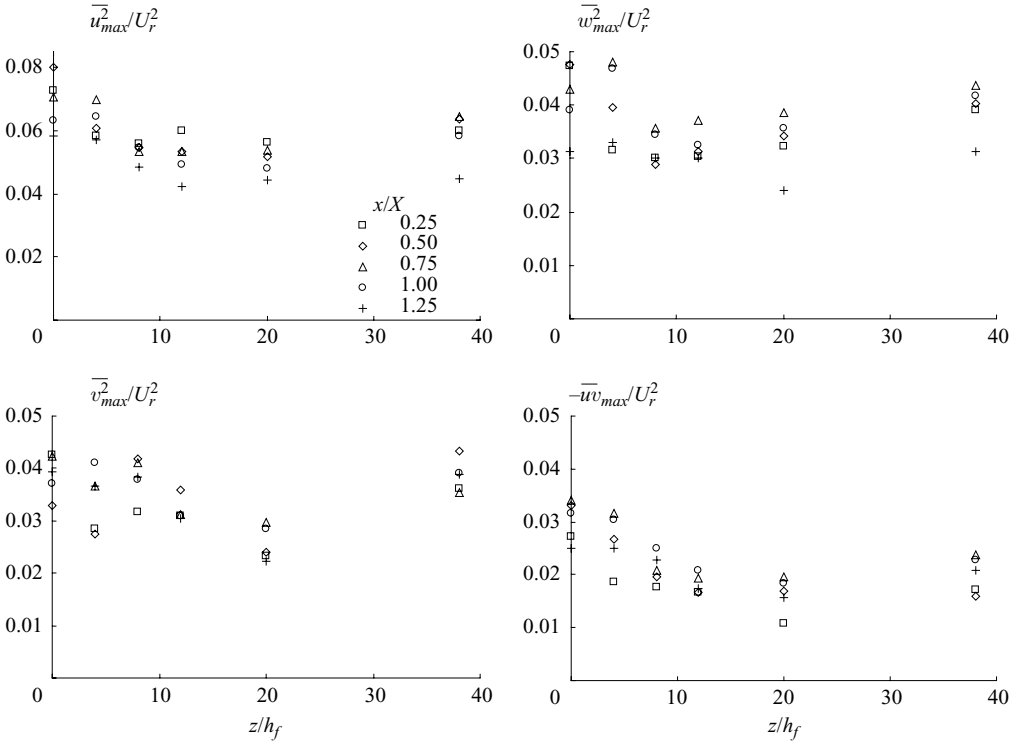

FIGURE 16. Peak levels of $\overline{u^2}$, $\overline{v^2}$, $\overline{w^2}$ and $-\overline{uv}$, variation with z/h_f.

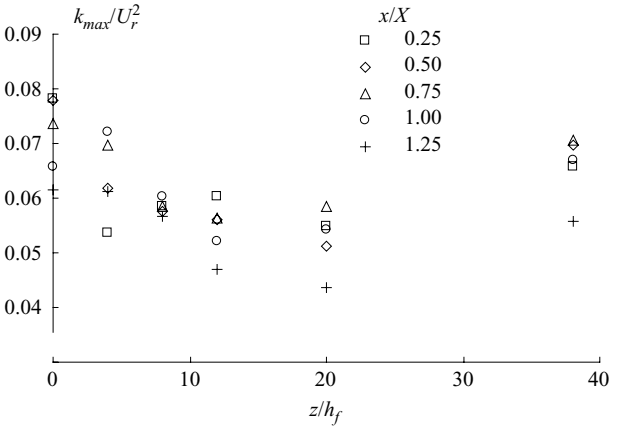

FIGURE 17. Variation of maximum turbulent kinetic energy with z/h_f. Note false origin.

3.3. *Strain rates*

The turbulence in the separation bubble is subjected to, in principle, all nine strain rates, and it is useful to consider some of these in relation to features seen in the turbulence. As a general point it should be remembered that the response to various strain rates is not a simple one, that the turbulence is generally not in a state of equilibrium with any particular strain rate unless the strain rate is sufficiently small.

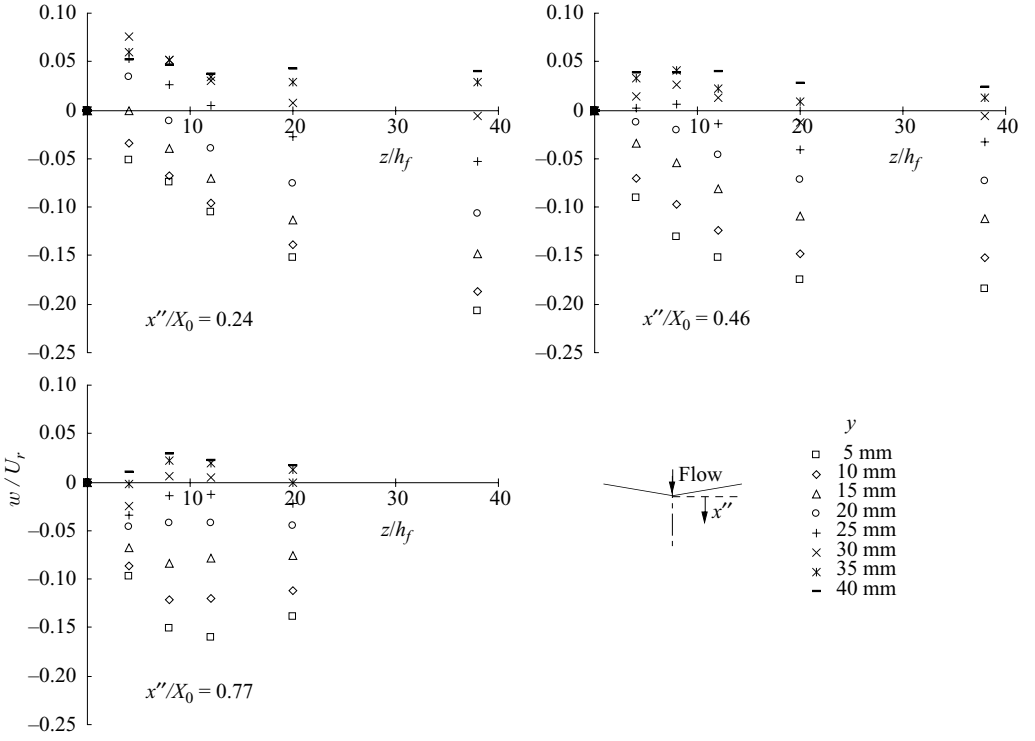

FIGURE 18. Variation of W/U_r with z/h_f at various heights y at three streamwise positions x''.

For convenience of discussion, the bubble can be divided into two parts – the 'central region' inside $z/h_f = 20$ and the 'intermediate region' between $z/h_f = 20$ and 38, where $z/h_f = 20$ corresponds to $z/X \sim 1$. This intermediate region could be regarded as a perturbation of the (nominally) spanwise-invariant flow further out. Here, the ratio of maximum strain rates, $(-\partial W'/\partial z')_{max}/(\partial U/\partial y)_{max}$, where W' and z' are parallel to the fence, is about 0.004, and shows the sensitivity of the turbulence levels to this strain rate, the stresses having decreased by roughly 20 %. In a spanwise-invariant region this ratio is zero, by definition.

In the central region the strain rates are more complex. Figure 18 shows profiles of W at fixed heights in 5 mm intervals (intervals of $0.019X_0$) against z, at three positions from the V apex. These have been obtained from interpolation of the profiles W given in figure 9. While $\partial W/\partial z$ is mostly negative everywhere, it is positive in the outer part of the flow near the centreline. The strength of this positive $\partial W/\partial z$ decreases with downstream distance, but the lateral extent over which it is positive moves outwards, because the peak in W moves outwards. Figure 21 shows V at the same intervals.

Figure 19 shows contours of strain rate, $\partial W/\partial z$, together with the locus of the shear-layer centreline defined by the height y_c, and the line of maximum k, on planes at $z = 0$ and $z/h_f = 4$. On and near $z = 0$, $\partial W/\partial z$ is *positive* over the shear layer centreline for the whole of the bubble length, and would account for the increase in Reynolds stresses. Figure 20 summarizes these plots in terms of $(\partial W/\partial z)/(\partial U/\partial y)$, where the gradients are evaluated where k is a maximum.

Now, of course, $\partial W/\partial z$ is not the only strain rate extra to $\partial U/\partial y$. Clearly, the shear layer is subjected to positive lateral divergence, but it is also curved, where the

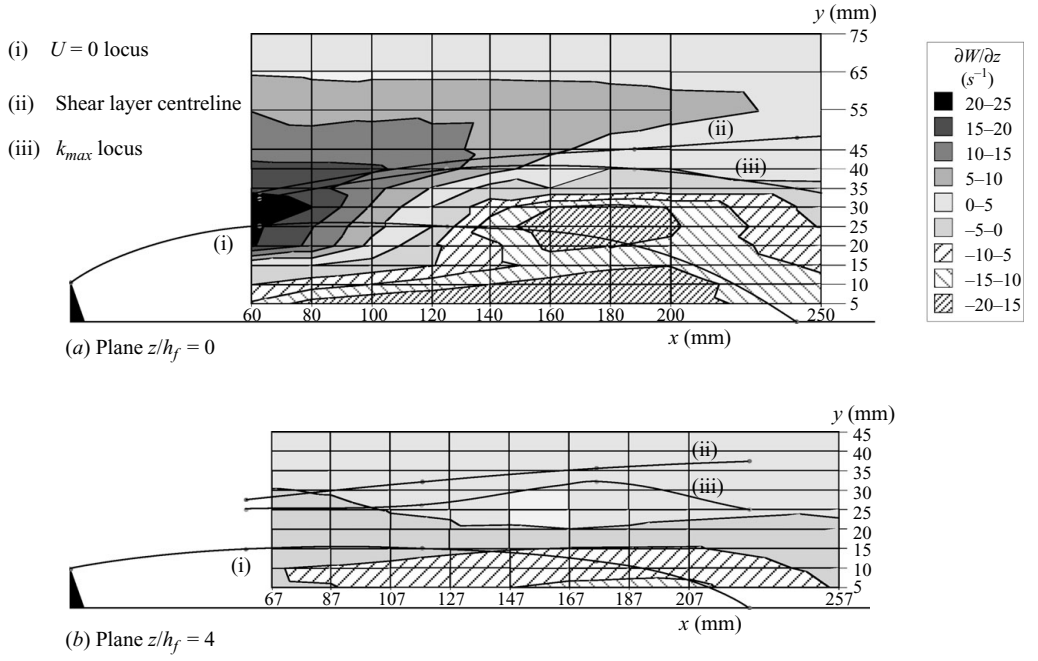

FIGURE 19. Contours of $\partial W/\partial z$ in planes at $z/h_f = 0$ and 4.

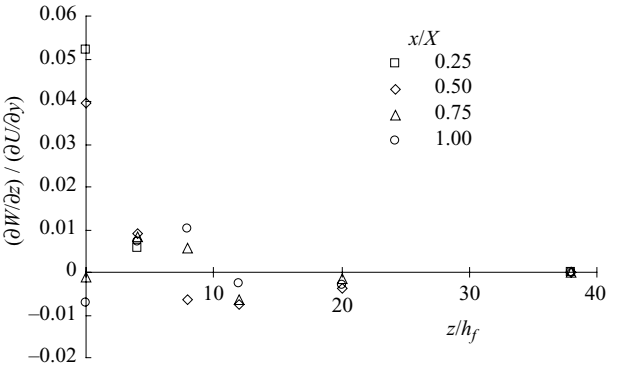

FIGURE 20. Variation of 'strain ratio' $(\partial W/\partial z)/(\partial U/\partial y)$ with z/h_f on the locus of k_{max}, at four streamwise stations x/X.

curvature of shear layer in the x–y plane can be described by $\partial V/\partial x$. Figure 22 shows $\partial W/\partial z$ and $\partial V/\partial x$ along the shear-layer centreline at, respectively, five and six lateral positions, where they have been normalized by $\partial U/\partial y$, also along the shear-layer centreline, to provide a proper measure of relative effect. In each case $(\partial V/\partial x)/(\partial U/\partial y)$ (figure 22*b*) is negative until near reattachment, implying a stabilizing sense of curvature, but of particular significance is the fact that there is very little difference between $(\partial V/\partial x)/(\partial U/\partial y)$ on one x–z plane and another. The slight variation that can be seen is comparable with the cumulative uncertainty in the measurements and calculation of the gradients. Thus, the curvature, and presumably the effects of curvature, do not vary significantly with z. Figure 22(*a*) shows $(\partial W/\partial z)/(\partial U/\partial y)$ reaches 0.05 at about $x = 0.4X_A$ on the centreline. Although this ratio decreases

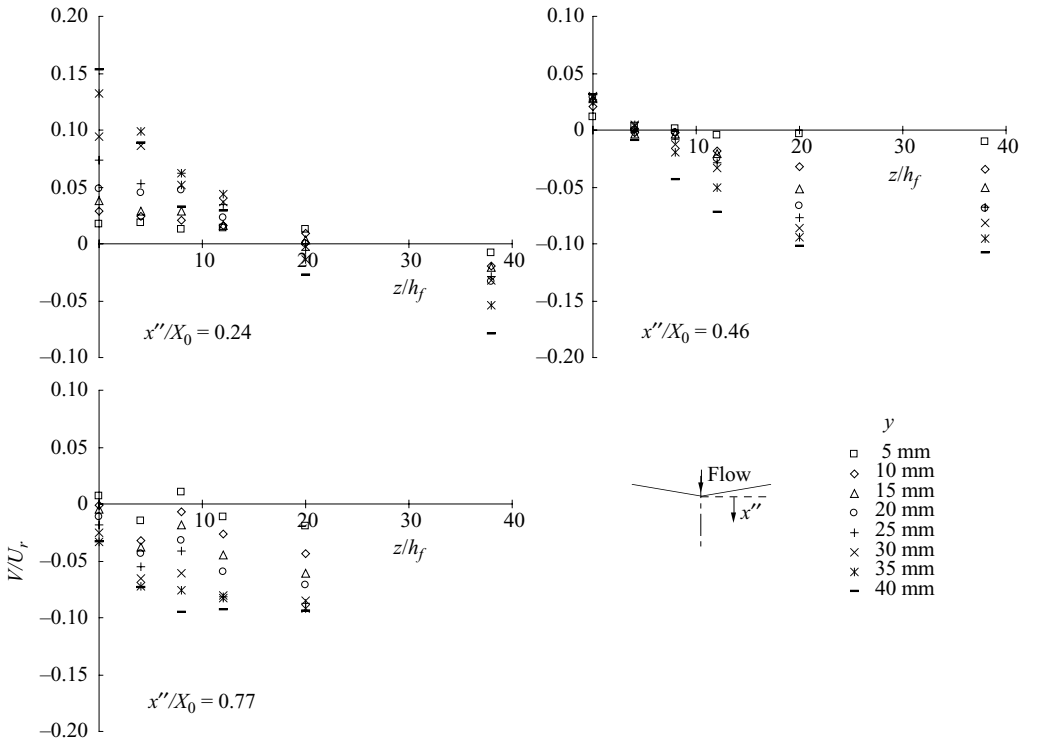

FIGURE 21. Variation of V/U_r with z/h_f at various heights y at three streamwise positions x''/X_0.

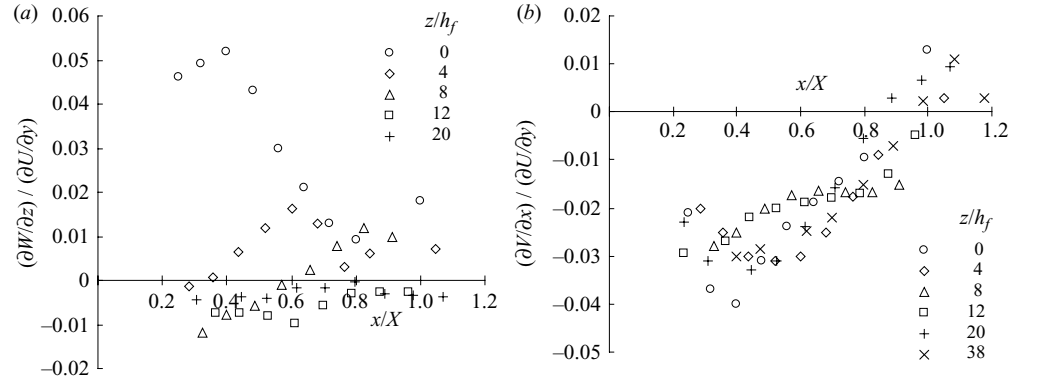

FIGURE 22. Variation of (*a*) $(\partial W/\partial z)/(\partial U/\partial y)$ and (*b*) $(\partial V/\partial x)/(\partial U/\partial y)$ on the shear layer centreline y_c with x/X.

substantially after this it nonetheless remains positive. A positive peak is seen on $z/h_f = 4$ at about $x = 0.6X_A$ and on $z/h_f = 8$ at about $x = 0.8X_A$, at which point $(\partial W/\partial z)/(\partial U/\partial y)$ is about the same positive level on each of the three in-most x–y planes (i.e. $z/h_f = 0$, 4 and 8). Further out $(\partial W/\partial z)/(\partial U/\partial y)$ is entirely negative.

Now $\partial V/\partial z$ is associated with the curvature of the shear layer in the y–z plane. Clearly, the curvature is not zero because of the central 'bulge' in the bubble. The magnitude of $\partial V/\partial z$ is comparable with the magnitude of $\partial W/\partial z$, as can

be inferred from figures 20 and 22. However, the effect of this type of curvature appears to be negligible, as is generally the case; boundary layers on the outside of a streamwise cylinder, for example, are very comparable to boundary layers on flat plates (Fernholz & Warnack 1998); the mixing layer on the edge of an axisymmetric (irrotational) jet, upstream of interaction is very close to that of a plane mixing layer (Johnson & Hancock 1991). As there is no clear indication to the contrary, the assumption here is that the effect of $\partial V/\partial z$ is negligible. Moreover, while the effects of $\partial V/\partial x$ can be linked to stabilizing or destabilizing effects of mean streamline curvature, there is not the same association with $\partial V/\partial z$ when, as here, the streamlines lie predominantly or entirely on x–y planes. The strain rate $\partial W/\partial z$ is of course linked to the other two direct strain rates, $\partial U/\partial x$ and $\partial V/\partial y$, through the continuity equation.

3.4. *Mixing layer scaling*

Qualitatively, the outer part of a separated flow is like a plane free shear layer, but subjected to fluctuating strain on its low speed side by the turbulence in the reverse flow, and to mean streamline curvature. However, as has been observed before, there is a degree of quantitative similarity, at least on the outer, 'high-speed' side, where the scaling is based on $(y - y_c)/L$ and $U_{max} - U_i$, for the velocity scale, where y_c and L were defined earlier. Figure 23 shows a comparison between the present measurements of turbulence kinetic energy and those of the mixing layer of Johnson & Hancock (1991). It can be seen there that there is close agreement with the mixing layer for $y > y_c$ over the first three-quarters of the bubble, independent of lateral position. Further downstream the peak levels become progressively larger than they are in the mixing layer, with a less extensive but still marked concurrence.

4. Concluding remarks

As mentioned in § 1, the overall intention was to set up a basis for improving the general understanding of the physics of three-dimensional separated flows where the flow is predominantly driven by Reynolds stress gradients. A specific aim of the work was to set up a separated and reattaching flow that had fully three-dimensional features, but had a systematic link to a two-dimensional (coplanar) counter part. Both the specific aim and the general intention have been achieved. At this juncture in the paper we merely wish to focus on some salient points.

The degree of the three-dimensionality might be described as *mild* in that the crossflow mean velocities were significantly less than the free-stream velocity. In the case here this velocity ratio was roughly 0.15. Even so, the effect was to increase the bubble height by a factor of roughly 1.7 (figure 4*b*) near attachment, and suggests that a *weak* crossflow would still have a significant effect, where weak might be a velocity ratio of, say, 0.02. If the relationship between height and velocity ratio were linear this would correspond to an increased height of about 10 %. For the present it is supposed that a strong degree of three-dimensionality would be when the velocity ratio is roughly unity, and very strong for a significantly larger ratio.

Even though the degree of three-dimensionality was *mild*, the effect on the mean flow and the turbulence structure was substantial. It remains to be seen how well this type of flow can be predicted and whether, for example, methods that do well in two-dimensional flow do well in this case. The flow was found to be symmetrical about the geometrical symmetry plane – a feature that was useful in the experiments – and could be subdivided for into two subregions, a central region and an intermediate region, inside the spanwise invariant region. In the latter of these two the flow was

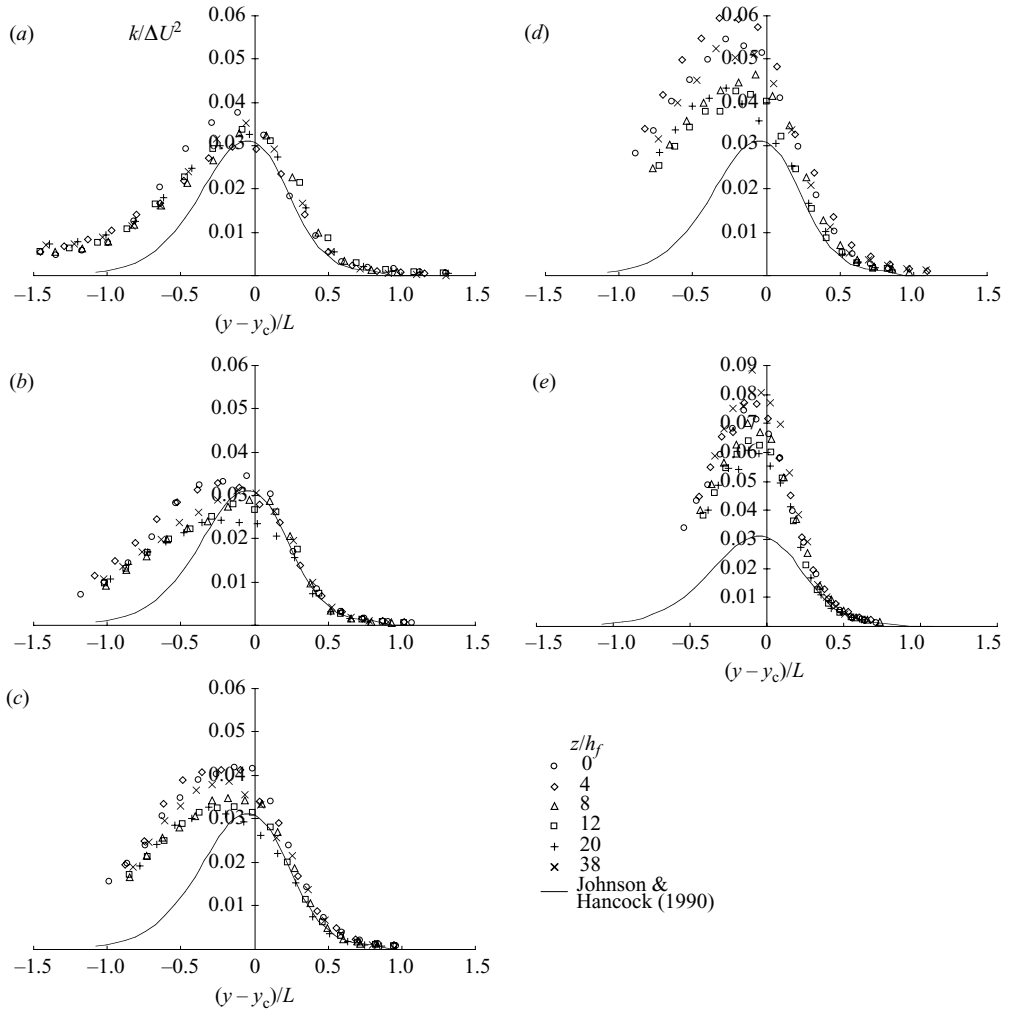

FIGURE 23. Turbulent kinetic energy k in plane mixing layer coordinates. (*a*) $x/X = 0.25$; (*b*) 0.5; (*c*) 0.75; (*d*) 1.0; (*e*) 1.25.

largely converging, making $\partial W/\partial z$ predominantly negative, and leading as would be anticipated to a suppression of the level of turbulence – it might be regarded as a perturbation of the spanwise-invariant region it adjoined. The central subregion extended laterally about one bubble length either side of the centreline, leading to substantial gradients in the lateral direction. It was marked by *increased* levels of turbulence, attributable at least in part to streamline divergence, that is, positive $\partial W/\partial z$, and a more complex flow structure. A distinctive feature was seen in the flow direction as inferred from velocity vectors in the x–z plane. The streamlines remained very nearly unchanged from the free-stream direction in the outer part of the overlying shear layer, that is, above about $2h_f$ (about $0.09X$). The same behaviour has been seen in a spanwise-invariant flow (Hancock & McCluskey 1996). Beneath this height there was a rapid change in direction which, as it happened, was largely independent of z.

A referee suggested that the variation in reattachment length seen here might depend on the stability of the laminar shear layer after separation. The inviscid analysis of

Huerre & Monkewitz (1985) shows that stability is controlled by the parameter $(U_1 - U_2)/(U_1 + U_2)$, where U_1 and U_2 are the free-stream velocities either side of the layer. (If it exceeds 1.315 a free shear layer is absolutely unstable and disturbances propagate upstream as well as downstream, or is convectively unstable.) The present shear layer is significantly different in that it is curved rather than planar, and is subjected to turbulent motions on its underside. The analysis of Alam & Sandham (2000) for a short separation bubble shows that the threshold for absolute instability increases from 1.15 with decreasing Reynolds number. Apart from noting that the above ratio varies between about 1.36 and 1.73 at the first station ($x/X = 0.25$), it is not possible to pursue this idea much further with the data available here.

The authors wish to thank Professor I. Castro for useful discussions during the course of the work, Mr A. Wells and Mr T. Laws for making the probes, Mr Wells for building the probe-traversing system and Mr T. Lawton for designing and building the driver electronics. We wish too to thank EPSRC for funding under grant GR/H78689, and QinetiQ (formerly DERA) under ASF/3061U.

REFERENCES

Adams, E. W. & Johnston, J. P. 1988 Flow structure in the near-wall zone of a turbulent separated flow. *AIAA J.* **26**, 932–939.

Alam, M & Sandham, N. D. 2000 Direct numerical simulation of 'short' laminar separation bubbles with turbulent reattachment. *J. Fluid Mech.* 403, 223–250.

Cao, C. 2002 The development of a three-dimensional turbulent separated flow downstream of reattachment. PhD Thesis, University of Surrey.

Cao, C. & Hancock, P. E. 2004 Boundary layer development after a region of three-dimensional separated flow. *Eur. J. Mech.* B/*Fluids* **23**, 519–533.

Castro, I. P. & Bradshaw, P. 1976 The turbulence structure of a distorted mixing layer. *J. Fluid Mech.* **73**, 265–304.

Castro, I. P. & Cheun, B. S. 1982 The measurement of Reynolds stresses with a pulsed-wire anemometer. *J. Fluid Mech.* **118**, 41–58.

Castro, I. P. & Dianat, M. 1990 Pulsed-wire anemometry near walls. *Exp. Fluids* **8**, 343–352.

Castro, I. P., Dianat, M. & Bradbury, L. J. S. 1987 The pulsed wire skin-friction measurement technique. In *Turbulent Shear Flows 5* (ed. F. Durst, B. E. Lauder, J. L. Lumley, F. W. Schmidt & J. H. Whitelaw), pp. 278–290. Springer.

Castro, I. P. & Epik, P. 1998 Boundary layer development after a separated region. *J. Fluid Mech.* **374**, 91–116.

Castro, I. P. & Haque, A. 1987 The structure of a turbulent separated shear layer bounding a separation region. *J. Fluid Mech.* **179**, 439–468.

Ciampoli, F. & Hancock, P. E. 2006 Effects of flow width in nominally two-dimensional turbulent separated flows. *Exp. Fluids* **40**, 196–202.

Dengel, P., Fernholz, H. H. & Hess, M. 1986 Skin-friction measurements in two- and three-dimensional highly turbulent flows with separation. In *Advances in Turbulence* (ed. G. Comte-Bellot & J. Mathieu), pp. 470–479. Springer.

Fernholz, H. H. 1994 Near-wall phenomena in turbulent separated flows. *Acta Mech.* **4**, Suppl., 57–67.

Fernholz, H. H. & Warnack, D. 1998 The effects of a favourable pressure gradient and of Reynolds number on an incompressible axisymmetric turbulent boundary layer. Part 1. The turbulent boundary layer. *J. Fluid Mech.* **359**, 329–356.

Hancock, P. E. 1999 Measurements of mean and fluctuating wall shear stress beneath spanwise-invariant separation bubbles. *Exp. Fluids* **27**, 53–59.

Hancock, P. E. 2000 Low Reynolds number two-dimensional separated and reattaching turbulent shear flow. *J. Fluid Mech.* **410**, 101–122.

Hancock, P. E. 2005 Velocity scales in the near-wall layer beneath reattaching turbulent separated and boundary layer flows. *Eur. J. Mech.* B/*Fluids* **24**, 425–438.

Hancock, P. E. 2007 Scaling of the near-wall layer beneath turbulent separated flow. *Eur. J. Mech.* B/*Fluids* **26**, 271–283.

Hancock, P. E. & Castro, I. P. 1993 End effects in nominally two-dimensional separated flows. *Appl. Sci. Res.* **51**, 173–178.

Hancock, P. E. & McCluskey, F. M. 1996 Spanwise-invariant three-dimensional separated flow. *Exp. Therm. Fluid Sci.* **14**, 25–34.

Hardman, J. R. 1998 Moderately three-dimensional separated and reattaching turbulent flow. PhD thesis, University of Surrey.

Hardman, J. R. & Hancock, P. E. 2000 The near-wall layer beneath a moderately converging three-dimensional turbulent separated and reattaching flow. *Eur. J. Mech.* B/*Fluids* **19**, 653–672.

Huerre, P. & Monkewitz, P. A. 1985 Absolute and convective instabilities in free shear layers. *J. Fluid Mech.* **159**, 151–168.

Jaroch, M. P. & Fernholz, H.-H. 1989 The three-dimensional character of a nominally two-dimensional separated and turbulent shear flow. *J. Fluid Mech.* **205**, 523–552.

Johnson, A. E. & Hancock, P. E. 1991 The effect of extra-strain rates of curvature and divergence on mixing layers. In *Turbulent Shear Flows 7* (ed. F. Durst, B. E. Lauder, W. C. Reynolds, F. W. Schmidt & J. H. Whitelaw) pp. 253–267. Springer.

Kaltenback, H-J. & Janke, G. 2000 Direct numerical simulation of flow separation behind a swept. Rearward-facing step at $Re_H = 3000$. *Phys. Fluids* **12**, 2320–2337.

Langston, L. S. & Boyle, M. T. 1982 A new surface flow-visualization technique. *J. Fluid Mech.* **125**, 53–57.

di Mare, L. & Jones, W. P. 2003 LES of turbulent flow past a swept fence. *Intl J. Heat Fluid Flow* **24**, 606–615.

McCluskey, F. M., Hancock, P. E. & Castro, I. P. 1991 Three-dimensional separated flows. In *Eighth Turbulent Shear Flows Symposium*, Munich, Germany, 9.5.1–9.5.6.

Na, Y. & Moin, P. 1998 Direct numerical simulation of a separated turbulent boundary layer. *J. Fluid Mech.* **374**, 379–405.

Patel, V. C. 1965 Calibration of the Preston tube and limitations on its use in pressure gradients. *J. Fluid Mech.* **23**, 185–208.

Perry, A. E. & Fairlie, B. D. 1974 Critical points in flow patterns. *Adv. Geophys.* B **18**, 299–315.

Poll, D. I. A. 1985 Some observtions of the transition process on the windward face of a long yawed cylinder. *J. Fluid Mech.* **150**, 329–356.

Ruderich, R. & Fernholz, H. H. 1986 An experimental investigation of a turbulent shear flow with separation, reverse flow, and reattachment. *J. Fluid Mech.* **163**, 283–322.

Schober, M., Hancock, P. E. & Siller, H. 1998 Pulsed-wire anemometry near walls. *Exp. Fluids* **25**, 343–352.

Song, S., de Graaff, D. B. & Eaton, J. K. 2000 Experimental study of a separating, reattaching, and redeveloping flow over a smoothly contoured ramp. *Intl J. Heat Fluid Flow* **21**, 512–519.

Sutton, E. P., Devenport, W. J. & Barkey Wolf, F. D. 1991 Experimental studies of the reattachment of separated shear layers. In *Separated Flows and Jets: IUTAM Symposium, Novosibirsk* (ed. V. V. Kozlov & A. V. Dovgal), pp. 573–588. Springer.

Yang, Z. & Voke, P. R. 2001 Large-eddy simulation of boundary layer separation and transition at a change of surface curvature. *J. Fluid Mech.* **439**, 305–333.